

## Appendix E

ATMOSPHERIC FATES OF CRIEGEE INTERMEDIATES IN  
THE OZONOLYSIS OF ISOPRENE

Nguyen, T. B., G. S. Tyndall, J. D. Crouse, A. P. Teng, K. H. Bates, R. H. Schwantes, M. M. Coggon, L. Zhang, P. Feiner, D. O. Miller, K. M. Skog, J. C. Rivera-Rios, M. Dorris, K. F. Olson, A. Koss, R. J. Wild, S. S. Brown, A. H. Goldstein, J. A. de Gouw, W. H. Brune, F. N. Keutsch, J. H. Seinfeld, and P. O. Wennberg (2016). "Atmospheric fates of Criegee intermediates in the ozonolysis of isoprene". In: *Phys. Chem. Chem. Phys.* 18.15, pp. 10241–10254. doi: 10.1039/C6CP00053C.

**Abstract**

We use a large laboratory, modeling, and field dataset to investigate the isoprene + O<sub>3</sub> reaction, with the goal of better understanding the fates of the C<sub>1</sub> and C<sub>4</sub> Criegee intermediates in the atmosphere. Although ozonolysis can produce several distinct Criegee intermediates, the C<sub>1</sub> stabilized Criegee (CH<sub>2</sub>OO, 61 ± 9%) is the only one observed to react bimolecularly. We suggest that the C<sub>4</sub> Criegees have a low stabilization fraction and propose pathways for their decomposition. Both prompt and non-prompt reactions are important in the production of OH (28% ± 5%) and formaldehyde (81% ± 16%). The yields of unimolecular products (OH, formaldehyde, methacrolein (42 ± 6%) and methyl vinyl ketone (18 ± 6%)) are fairly insensitive to water, *i.e.*, changes in yields in response to water vapor (≤4% absolute) are within the error of the analysis. We propose a comprehensive reaction mechanism that can be incorporated into atmospheric models, which reproduces laboratory data over a wide range of relative humidities. The mechanism proposes that CH<sub>2</sub>OO + H<sub>2</sub>O ( $k_{(H_2O)} \sim 1 \times 10^{-15} \text{ cm}^3 \text{ molec}^{-1} \text{ s}^{-1}$ ) yields 73% hydroxymethyl hydroperoxide (HMHP), 6% formaldehyde + H<sub>2</sub>O<sub>2</sub>, and 21% formic acid + H<sub>2</sub>O; and CH<sub>2</sub>OO + (H<sub>2</sub>O)<sub>2</sub> ( $k_{(H_2O)_2} \sim 1 \times 10^{-12} \text{ cm}^3 \text{ molec}^{-1} \text{ s}^{-1}$ ) yields 40% HMHP, 6% formaldehyde + H<sub>2</sub>O<sub>2</sub>, and 54% formic acid + H<sub>2</sub>O. Competitive rate determinations ( $k_{SO_2}/k_{(H_2O)_{n=1,2}} \sim 2.2 (\pm 0.3) \times 10^4$ ) and field observations suggest that water vapor is a sink for greater than 98% of CH<sub>2</sub>OO in a Southeastern US forest, even during pollution episodes ([SO<sub>2</sub>] ~ 10 ppb). The importance of the CH<sub>2</sub>OO + (H<sub>2</sub>O)<sub>n</sub> reaction is demonstrated by high HMHP mixing ratios observed over the forest canopy. We find that CH<sub>2</sub>OO does not substantially affect the lifetime of SO<sub>2</sub> or HCOOH in the Southeast US, *e.g.* CH<sub>2</sub>OO + SO<sub>2</sub> reaction is a minor contribution

(<6%) to sulfate formation. Extrapolating, these results imply that sulfate production by stabilized Criegees is likely unimportant in regions dominated by the reactivity of ozone with isoprene. In contrast, hydroperoxide, organic acid, and formaldehyde formation from isoprene ozonolysis in those areas may be significant.

## E.1 Introduction

Ozonolysis is one of the main atmospheric oxidation pathways for volatile alkenes. Reaction with ozone globally removes ~10% of isoprene (C<sub>5</sub>H<sub>8</sub>), the most abundant alkene in the atmosphere. For monoterpenes (C<sub>10</sub>H<sub>16</sub>) and sesquiterpenes (C<sub>15</sub>H<sub>24</sub>), ozonolysis is a substantially larger sink due to their faster rate coefficients with ozone (Atkinson *et al.*, 2006). The first steps of the alkene ozonolysis mechanism are shown in Figure E.1 (Criegee, 1975). Two primary ozonides (POZ) are formed from ozone addition at either double bond of isoprene, decomposing into methacrolein (MACR), methyl vinyl ketone (MVK), formaldehyde (HCHO), and potentially up to nine activated Criegee intermediates (CI, denoted with asterisk). The C<sub>4</sub> Criegees (MACR-OO\* and MVK-OO\*) can be formed with four conformations each that are *syn* or *anti* to methyl or vinyl groups. The CI can experience a few unimolecular processes – most notably, decomposition into a hydroxyl radical (OH) and a β-oxy alkyl radical (R) and thermalization by atmospheric gases to form the stabilized Criegee intermediate (SCI) (Kroll *et al.*, 2001). In addition, a fraction of SCI has been suggested to be formed through POZ decomposition (Drozd and Donahue, 2011). Most of the OH from isoprene ozonolysis is thought to be produced by the *syn*-methyl MVK-OO conformers (Figure E.1, g and h) *via* the formation of a vinyl hydroperoxide (VHP) intermediate (Aschmann and Atkinson, 1994; Donahue *et al.*, 2011; Gutbrod *et al.*, 1997; Kuwata *et al.*, 2010; Paulson *et al.*, 1992).

The stabilized Criegees (SCIs) may undergo bimolecular reaction with a number of atmospheric species, including water vapor (H<sub>2</sub>O), sulfur dioxide (SO<sub>2</sub>), formic acid (HCOOH), carbonyls (*e.g.* HCHO and acetaldehyde), NO, NO<sub>2</sub>, O<sub>3</sub>, RO<sub>2</sub>, alkenes, among others (Fenske *et al.*, 2000; Hatakeyama and Akimoto, 1994; Johnson and Marston, 2008; Kjaergaard *et al.*, 2013; Neeb *et al.*, 1998; Vereecken *et al.*, 2012, 2014). Even if a substantial fraction of CIs are stabilized, they may still experience unimolecular losses. The structure, and even conformation, of the SCI dictate their unimolecular and bimolecular reactivities (Gutbrod *et al.*, 1997), with *syn* SCI more susceptible to decomposition. The simplest SCI (CH<sub>2</sub>OO) has special importance in atmospheric chemistry as it is produced by all exocyclic alkenes, including isoprene. Unlike other SCIs, however, CH<sub>2</sub>OO is non-*syn* (*i.e.*, not facing any

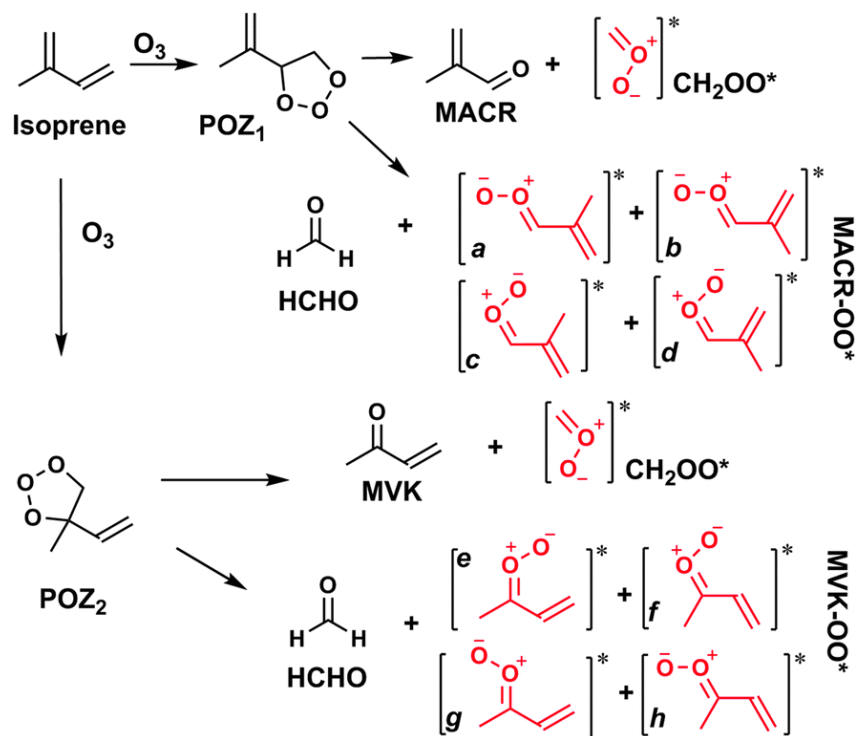


Figure E.1: The first steps of the Criegee mechanism of ozonolysis, shown for isoprene. Criegee intermediates are drawn as zwitterions; however, depending on the chemical structure, they may also have diradical character.

hydrocarbon groups), which greatly reduces its unimolecular reactivity (Anglada *et al.*, 2011).

Figure E.2 shows a simplified reaction scheme between  $CH_2OO$  and water (or water clusters) (Berndt *et al.*, 2014; Chao *et al.*, 2015; Ryzhkov and Ariya, 2003, 2006), sulfur dioxide ( $SO_2$ ), and formic acid ( $HCOOH$ ). The  $CH_2OO + (H_2O)_n$  reaction (where  $n = 1, 2, \dots$ ) produces hydroxymethyl hydroperoxide (HMHP), hydrogen peroxide ( $H_2O_2$ ) + formaldehyde ( $HCHO$ ), and formic acid ( $HCOOH$ ) +  $H_2O$  as main products (Becker *et al.*, 1993; Gab *et al.*, 1985; Horie *et al.*, 1994a; Huang *et al.*, 2013; Neeb *et al.*, 1995, 1997; Ryzhkov and Ariya, 2004). The  $CH_2OO + HCOOH$  reaction produces hydroperoxy methylformate (HPMF) (Neeb *et al.*, 1995, 1997; Thamm *et al.*, 1996). Finally, the  $CH_2OO + SO_2$  reaction produces  $SO_3$ , which then reacts with water to form  $H_2SO_4$  (Hatakeyama *et al.*, 1984).

Certain populations of SCIs may produce OH (Novelli *et al.*, 2014), perhaps analogously to the hot Criegee VHP channel, among other products. Decomposition of SCIs is rarely discussed within the scope of the atmospheric fates; however, it is an

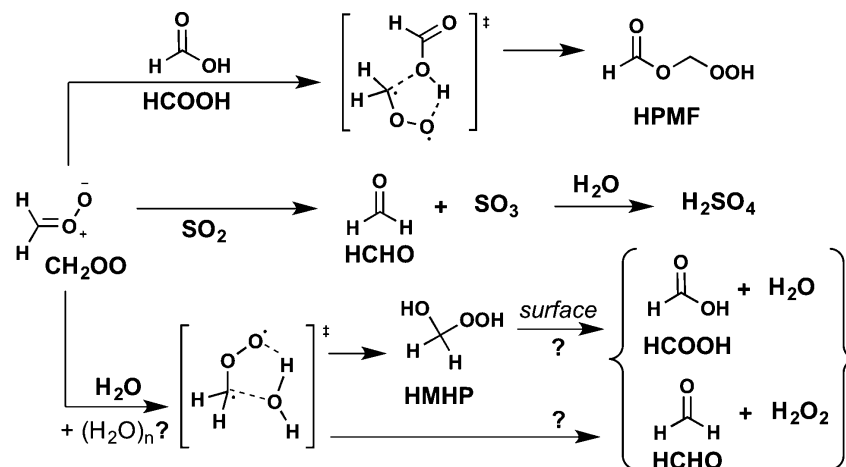


Figure E.2: The reaction of  $\text{CH}_2\text{OO}$  with  $\text{HCOOH}$ ,  $\text{SO}_2$ , and  $\text{H}_2\text{O}$  (and possibly water clusters). The production of  $\text{HCOOH} + \text{H}_2\text{O}$  and  $\text{HCHO} + \text{H}_2\text{O}_2$  from the water reaction has been suggested to (at least partially) result from surface-mediated decomposition of HMHP (Neeb *et al.*, 1997); however, it is not clear if there are direct routes to these products from  $\text{CH}_2\text{OO} + \text{H}_2\text{O}$ .

important consideration in understanding their total reactivity. Previously published unimolecular decomposition rates for larger Criegees have high uncertainty, so the following is only a qualitative discussion. SCI decomposition rates has been shown to increase with size (Fenske *et al.*, 2000; Newland *et al.*, 2015). For example, even though the thermalized acetone oxide ( $(\text{CH}_3)_2\text{COO}$ ) has been recently reported to undergo a diffusion-limited reaction with  $\text{SO}_2$  (Huang *et al.*, 2015), its short unimolecular lifetime due to its all-*syn* conformation, *i.e.*, both sides facing methyl groups, severely limits the atmospheric relevance of its bimolecular reactions ( $\tau_{uni} = 0.001\text{--}0.004$  s) (Huang *et al.*, 2015; Newland *et al.*, 2015; Olzmann *et al.*, 1997). It should be noted that experimental determinations of unimolecular lifetimes (*e.g.* 0.002 s) may have some contribution from Criegee self-reaction (Huang *et al.*, 2015); thus,  $\tau_{uni}$  may be closer to the higher end of the reported range. The ratio  $k_{decomp}/k_{\text{SO}_2}$  for *syn*- $\text{CH}_3\text{CHOO}$  and  $(\text{CH}_3)_2\text{COO}$  have been measured to be 1 and 2 orders of magnitude higher than that for  $\text{CH}_2\text{OO}$ , respectively (Newland *et al.*, 2015). Thus, even in a polluted atmosphere ( $\sim 10$  ppb  $\text{SO}_2$  and 50% RH at room temperature), decomposition using the Olzmann *et al.* (1997) lower-limit rate coefficient accounts for the majority ( $\sim 76\%$ ) of the acetone oxide fate, while the reaction with  $\text{SO}_2$  is minor ( $\sim 8\%$ ). The Newland *et al.* (2015) relative rate coefficient (using  $k_{\text{SO}_2}$  of Huang *et al.*, 2015) predicts an even higher decomposition fraction.

The present work focuses on understanding the bimolecular reactive channels of  $\text{CH}_2\text{OO}$  and, more generally, the mechanism of isoprene ozonolysis in the atmosphere. We neglect the unimolecular reactions for  $\text{CH}_2\text{OO}$ , as it has a long lifetime with respect to decomposition at 298 K and 1 atm ( $\sim 3$  s) (Olzmann *et al.*, 1997). Furthermore, we provide suggestions for a unifying reaction scheme that may be incorporated into atmospheric models.

## E.2 Experimental Methods

### E.2.1 Chamber Methods

Experiments were conducted in the Caltech dual 24 m<sup>3</sup> Teflon environmental chambers at  $\sim 295$  K and  $\sim 1$  atm. A subset of the work was performed as part of the FIXCIT campaign and the overview manuscript (Nguyen *et al.*, 2014b) provides an in-depth description of the chamber and relevant experiments. Product yield studies were investigated with isoprene and ozone mixing ratios of  $\sim 100$  and 600 ppb, respectively, and relative humidity (RH) in the approximate range of  $<4 - 76\%$ . The production of OH was investigated in the absence of a chemical scavenger, but all other studies were performed with excess cyclohexane (50 ppm) to scavenge OH. Although excess cyclohexane is used, a minor fraction of the products will result from OH chemistry. Relative rate experiments were used to investigate the competition between  $\text{SO}_2$  and  $\text{H}_2\text{O}$  at lower isoprene and ozone mixing ratios ( $\sim 25$  ppb and 100 ppb, respectively) and 10 ppm cyclohexane.

RH inside the reaction chambers was adjusted to the desired level at the beginning of each experiment with a Nafion membrane humidifier (Permapure, LLC) and recirculating ultra-purified water (Millipore Milli-Q, 18 M $\Omega$ ,  $<3$  ppb TOC). The RH was stable throughout each experiment, as verified by a Vaisala HMT221 probe that was calibrated in the range of 11–95% with saturated salt solutions. Water vapor in the range of  $\text{RH} < 10\%$  was measured by chemical ionization mass spectrometry (CIMS, see Section E.2.2). However, the accuracy of RH measurements degrades in the lower range due to the difficulty in determining small mixing ratios of  $\text{H}_2\text{O}$ ; thus we quote "dry" RH as " $<4\%$ ". Although RH in dry conditions is quoted as an upper bound, we estimate the actual RH in the chamber is closer to 1%. Ozone was introduced into the chamber by flowing air through a commercial UV ozone generator. Reagents, *e.g.* isoprene (Aldrich,  $\geq 99\%$ ) and cyclohexane (CHX, Aldrich  $>99\%$ ), were introduced into the chamber by volumetric injection of liquid material using Hamilton gas-tight syringes. In general, the order of introduction was water vapor, ozone, cyclohexane, and then isoprene. For relative rate studies, gaseous  $\text{SO}_2$

(standard mixture 10 ppm in N<sub>2</sub>, Scott Specialty Gases) was introduced into the chamber using a calibrated mass flow controller. After injection of isoprene, several short high-pressure pulses of air were introduced into the chamber to homogenize the contents of the chamber so that the reaction can start immediately and uniformly. We verified that injected gases were well-mixed in <5 minutes using this method. The duration of a typical experiment was 5–7 hours.

### E.2.2 Analytical Quantification

isoprene, methacrolein (MACR), methyl vinyl ketone (MVK), and cyclohexane (CHX) were quantified by gas chromatography with a flame ionization detector (GC-FID). The GC-FID was calibrated with commercial standards (Aldrich) in the range of 20–200 ppb by use of volumetric gas-tight syringes and a calibrated mass flow of N<sub>2</sub> into a 100L Teflon calibration bag. Additionally, the absolute quantities of ISOP, MACR, and MVK was cross calibrated using Fourier transform infrared spectroscopy (FT-IR) in the range of 1–20 ppm *via* a similar method. The ppm-level calibration bags were quantified with FT-IR using tabulated absorption cross sections (Sharpe *et al.*, 2002) before sampling with GC-FID. The mixing ratio of ozone was quantified by a calibrated ozone absorption monitor (Horiba APOA-360). The mixing ratios of NO and NO<sub>2</sub> were quantified with a commercial NO<sub>x</sub> monitor (Teledyne T200). NO was observed at baseline level (limit of detection 0.5 ppb) and NO<sub>2</sub> remained below 5 ppb during ozonolysis experiments. Sulfuric acid aerosols were measured using a time-of-flight aerosol mass spectrometer (AMS, Aerodyne) and data processing was performed using the Pika 1.14D analysis module in Igor Pro (Drewnick *et al.*, 2005). The instrumental ionization efficiency was calibrated with 350 nm ammonium nitrate particles.

Formaldehyde and HO<sub>x</sub> (OH and HO<sub>2</sub>) were measured in situ by two laser-induced fluorescence (LIF) instruments during the FIXCIT campaign. The University of Wisconsin (UW) LIF instrument (DiGangi *et al.*, 2011; Hottle *et al.*, 2009) quantified formaldehyde from the difference between its online (353 nm) and offline signal. The Pennsylvania State University (PSU) Ground-based Tropospheric Hydrogen Oxides Sensor (GTHOS (Brune *et al.*, 1995)) measured OH and HO<sub>2</sub> by the fluorescent assay by gas expansion (FAGE) technique. OH was quantified spectroscopically (near 308 nm) and the zero background is determined using hexafluoropropene (C<sub>3</sub>F<sub>6</sub>) as an OH scrubber in the instrument inlet. HO<sub>2</sub> was measured after its chemical conversion in the instrument inlet to OH using pure NO (HO<sub>2</sub> + NO → OH + NO<sub>2</sub>). The known interference of HO<sub>2</sub> measurement by RO<sub>2</sub> radicals (Fuchs

*et al.*, 2011) was corrected in the following manner: the NO addition to GTHOS was modified to reduce the reaction time and the amount of NO added. Although the conversion of HO<sub>2</sub> to OH was decreased from ~90% to less than 10%, the conversion of RO<sub>2</sub> to OH was reduced to less than 1%, so that more than 95% of the signal was due to converted HO<sub>2</sub> and only a few percent was due to RO<sub>2</sub> (Fuchs *et al.*, 2011). These conversion rates were measured with GTHOS in the Brune laboratory at PSU and are similar to those determined by Fuchs *et al.* (2011).

Gas-phase hydroperoxides (H<sub>2</sub>O<sub>2</sub>, HMHP, MHP, *etc.*), acidic compounds (SO<sub>2</sub>, HCOOH, *etc.*), and other volatiles with more than one polar functional group (*e.g.* hydroxy carbonyls) are quantified with a triple-quadrupole chemical ionization mass spectrometer (CIMS) using CF<sub>3</sub>O<sup>-</sup> as an ionization reagent (Crouse *et al.*, 2006; St. Clair *et al.*, 2010). The sample flow from the chamber was diluted by a factor of 12 with dry N<sub>2</sub> before mass spectrometry analysis. The dry (RH < 4%) sensitivity of triple-quadrupole CF<sub>3</sub>O<sup>-</sup> CIMS to different analytes was cross-calibrated with a CF<sub>3</sub>O<sup>-</sup> time-of-flight (ToF) CIMS during the FIXCIT campaign. The ToF CIMS was calibrated for a variety of compounds (H<sub>2</sub>O<sub>2</sub>, HMHP, HCOOH, SO<sub>2</sub>, peracetic acid (PAA), acetic acid (AA), hydroxyacetone (HAC), *etc.*) with commercial or synthesized standards based on gravimetric or spectrometric techniques (see Section S3 of Nguyen *et al.* (2015a) for more information). Table E.2 in the Supporting Information provides more information about CIMS detection of the major compounds discussed in this work. The CIMS measurement uncertainties are approximately 20–30% for calibrated compounds (*e.g.* HCOOH) and ~50% for uncalibrated compounds (*e.g.* HPMF).

In addition to the dry sensitivity, the dependence of the ion chemistry on water vapor is unique to each CIMS instrument and is critical for the accurate interpretation of RH-dependent yields. We obtained the water-dependent calibration curves in the experimental RH range by introducing a sample stream (containing a stable gaseous source of each compound) and a dilution stream that has tunable water vapor content to the CIMS flow tube region. The water vapor mixing ratio of the dilution stream was achieved by mixing flow-controlled quantities of a humid air stream ([H<sub>2</sub>O] ~ 3%, quantified by FT-IR) and a dry N<sub>2</sub> stream ([H<sub>2</sub>O] < 100 ppm). A stable source of HMHP, for which a commercial standard is unavailable, was synthesized in the Teflon chamber using the HCHO + HO<sub>2</sub> reaction (Niki *et al.*, 1980), which produces a low yield of HMHP. The photolysis of HCHO (~2 ppm) generates the HO<sub>2</sub> that is needed to react with HCHO. The UV lights were turned off after approximately

1 hour, and the ~6 ppb HMHP formed during the photolytic period was stable in the dark indefinitely. A typical water-dependent calibration alternates a dry data point with several humid points and zeros (where sample flow is shut off), after each period is allowed to stabilize (Figure E.9 in the Supporting Information). Water curves were obtained for HCOOH, H<sub>2</sub>O<sub>2</sub>, and SO<sub>2</sub> using commercial standards as the sample source, in an identical manner. The sensitivity of the CIMS toward HPMF was not measured, but was assumed to be similar to HMHP based on the molecular characteristics of these two compounds (Su and Chesnavich, 1982).

### E.2.3 Wall loss Corrections

$\alpha$ -hydroxy hydroperoxides like HMHP have a propensity to participate in heterogeneous reactions on humid surfaces (Neeb *et al.*, 1997). Thus, we measured wall loss rates for HMHP, HCOOH, and H<sub>2</sub>O<sub>2</sub> as a function of RH to correct for this effect. HMHP was synthesized *via* an alternative method to the one described in Section E.2.2: a gaseous mixture of formaldehyde/N<sub>2</sub> (produced by flowing dry N<sub>2</sub> past heated paraformaldehyde solid) was bubbled into an aqueous H<sub>2</sub>O<sub>2</sub> solution (50% v/v). The outflow of the bubbler (containing HCHO, HMHP, HCOOH, and H<sub>2</sub>O<sub>2</sub>) was introduced into the chamber until the signal of HMHP in CIMS was adequate, after which the flow was stopped and the wall loss was monitored for 8–10 hours. The production of HCOOH from HMHP conversion may obscure the HCOOH wall loss to a degree. However, by virtue of the synthesis method (high water content in the H<sub>2</sub>O<sub>2</sub> bubbler), the HCOOH mixing ratio in the chamber was more abundant than HMHP by a factor of 100, so that even if all of the HMHP were converted to HCOOH, the production yield signal would impact  $k_{wall}$  of HCOOH by only 1%. We did not observe noticeable wall loss of HMHP, HCOOH, or H<sub>2</sub>O<sub>2</sub> under dry conditions (Figure E.10 in the Supporting Information); however, the wall loss rates become non-negligible at the highest RH investigated (72%), where HMHP was removed at a rate of approximately 0.1% per minute. The humidity-dependent wall loss rates ( $k_{wall, HMHP} = -1.4 \times 10^{-5} \times RH \text{ min}^{-1}$ ,  $k_{wall, H_2O_2} = -9.6 \times 10^{-6} \times RH \text{ min}^{-1}$ , and  $k_{wall, HCOOH} = -2.2 \times 10^{-6} \times RH \text{ min}^{-1}$ ) were used to correct the CIMS data.

## E.3 Results and Discussion

### E.3.1 Humidity-Dependent Product Yields

The molar yields of products from the isoprene ozonolysis in the RH range of <4–76% are reported in Table E.1. Figure E.3 shows the trends in yields of select gas-

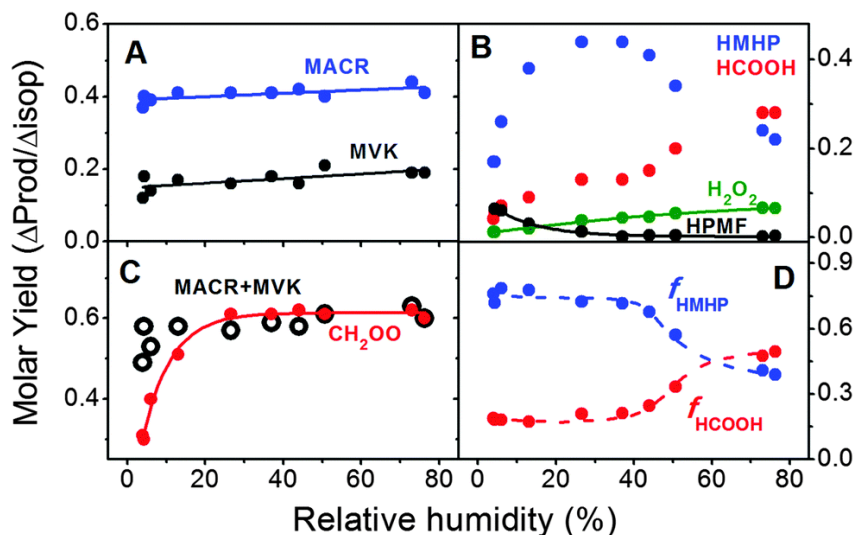


Figure E.3: Molar yields of the isoprene + O<sub>3</sub> reaction products (A–C) at several RH conditions. The CH<sub>2</sub>OO yield in panel C is inferred from the sum of the scavenged products of CH<sub>2</sub>OO with water vapor and formic acid. Panel D shows the fraction of water-scavenged CH<sub>2</sub>OO that is observed as HMHP ( $f_{HMHP}$ ) and HCOOH ( $f_{HCOOH}$ ). Solid lines indicate least-squares fits, when applicable, and dashed lines only serve to guide the eyes. HMHP and HCOOH in panel B can each be fit by two exponential curves delineated at RH ~40%, but no singular relationship.

phase organic products measured by GC-FID and CIMS. As expected, the "prompt" products, *i.e.*, those formed primarily from the decomposition of primary ozonides (POZ) such as HCHO, MACR, and MVK, do not exhibit a strong dependence on water vapor (Figure E.3a and Table E.1). This is also true for yields of OH radicals, which are produced from decomposition channels. The observation that OH yields from isoprene ozonolysis are independent of humidity has been reported in other works (Hasson *et al.*, 2003; Kuwata *et al.*, 2010). Further insights on the sources of OH and HCHO yields are obtained by model simulations (see Section E.3.2). The yields of carbonyls and OH from this work are not significantly different from those reported elsewhere (Aschmann and Atkinson, 1994; Atkinson *et al.*, 1992; Grosjean *et al.*, 1993b; Gutbrod *et al.*, 1997; Hasson *et al.*, 2001a; Sauer *et al.*, 1999). The trends in yields for carbonyls are slightly positive with humidity, possibly supporting a minor production from SCI + (H<sub>2</sub>O)<sub>*n*</sub> reaction (H<sub>2</sub>O<sub>2</sub> as coproduct). However, the measurement uncertainties are significant (10-30%) and, thus, this channel was treated as minor in the development of our mechanism.

Stabilized CH<sub>2</sub>OO yields obtained by a chemical scavenging method were similar whether H<sub>2</sub>O or SO<sub>2</sub> was used as the Criegee scavenger (Table E.1,  $Y_{SCI} \sim 0.60$

expt.	type	SO <sub>2</sub> (ppb)	RH (%)	Y <sub>CH<sub>2</sub>OO</sub>	Y <sub>MACR</sub>	Y <sub>MVK</sub>	Y <sub>OH</sub>	Y <sub>HCHO</sub>	Y <sub>HCO<sub>2</sub>H</sub>	Y <sub>H<sub>2</sub>O<sub>2</sub></sub>	Y <sub>HMHP</sub>	Y <sub>HPMF</sub>
1	A	0	<4	0.30	0.39	0.15	—	0.79	0.05	0.012	0.17	0.064
2	A	0	6	0.40	0.39	0.14	—	—	0.07	0.014	0.26	0.060
3	A	0	13	0.51	0.41	0.17	—	—	0.09	0.019	0.38	0.030
4	A	0	27	0.61	0.41	0.16	—	—	0.13	0.038	0.44	0.013
5	A	0	37	0.61	0.41	0.18	—	0.83	0.13	0.044	0.44	0.001
6	A	0	44	0.62	0.42	0.16	—	-0.15	0.046	0.41	0.005	—
7	A	0	51	0.61	0.40	0.21	—	—	0.20	0.054	0.34	0.004
8	A	0	73	0.62	0.44	0.19	—	—	0.28	0.066	0.24	0.002
9	A	0	76	0.60	0.41	0.19	—	—	0.28	0.065	0.22	0.003
10	B	0	4	—	—	—	0.28	—	—	—	—	—
11	B	0	52	—	—	—	0.28	—	—	—	—	—
12	C	15	20	0.60	BDL	BDL	—	—	—	—	—	—
13	C	15	3	0.65	BDL	BDL	—	—	—	—	—	—
14	C	75	3	0.66	BDL	BDL	—	—	—	—	—	—

Table E.1: Molar yields ( $Y$ ) of major products for different RH and SO<sub>2</sub> conditions. Experiment types are (A) product yields with OH scavenger ([ISO] ~100 ppb, [O<sub>3</sub>] ~600 ppb, [CHX] ~50 ppb), (B) product yields without OH scavenger (same initial conditions as A but without CHX), and (C) relative rates ([ISO] ~25 ppb, [O<sub>3</sub>] ~120 ppb, [CHX] ~10 ppm). CH<sub>2</sub>OO yields for A are obtained by summing the yields of CH<sub>2</sub>OO + (H<sub>2</sub>O)<sub>n</sub> and CH<sub>2</sub>OO + HCOOH products measured using CIMS. In C, CH<sub>2</sub>OO yield determinations include the measurement of H<sub>2</sub>SO<sub>4</sub> aerosol using AMS. All experiments were performed at 295 K. See Table E.2 in the Supporting Information for details on quantification with CIMS. Missing entries indicate unavailability of instruments or irrelevancy of data. Measurement uncertainties are: SO<sub>2</sub> (±20%), CH<sub>2</sub>OO (±15 AMS, ±30% CIMS), MACR (±15%), MVK (±33%), OH (±25%), HCHO (±20%), HCOOH (±10%), H<sub>2</sub>O<sub>2</sub> (±20%), HMHP (±20%), HPMF (±50%). BDL = below detection limit for GC-FID.

using CIMS, and  $\sim 0.64$  using AMS). As the detection of scavenged products utilized two independently-calibrated instruments, their agreement lends further confidence to the yield results. Our  $\text{CH}_2\text{OO}$  determination is consistent, within uncertainties, with those reported recently (0.56–0.60) (Newland *et al.*, 2015; Sipilä *et al.*, 2014). However, it is in poor agreement with the 0.27 yield determined by Hasson *et al.* (2001a). We believe the discrepancy is due to the fact that  $\text{HCOOH}$  and  $\text{H}_2\text{O}_2$  were not counted as  $\text{CH}_2\text{OO} + (\text{H}_2\text{O})_n$  products in the Hasson *et al.* (2001a) work, and the offline HMHP determination may have experienced aqueous losses. The  $\text{CH}_2\text{OO}$  yield reported here is supported by independent observations of its co-products, MVK and MACR (Figure E.1). Figure E.3c shows that the  $\text{CH}_2\text{OO}$  yield determined here is in good agreement with the  $\text{C}_4$  carbonyl sum at high water vapor mixing ratios where  $\text{CH}_2\text{OO}$  is fully scavenged. The inferred  $\text{CH}_2\text{OO}$  yield in our work does not include formaldehyde as a product due to limited data. Formaldehyde formation becomes important at low RH because of competing reactions such as  $\text{CH}_2\text{OO} + \text{O}_3$ ; thus, a significant deviation in the inferred  $\text{CH}_2\text{OO}$  yield compared to the  $\text{C}_4$  carbonyl sum occurs in the low RH range.

The products derived from  $\text{CH}_2\text{OO}$  bimolecular reactions have a strong relationship with water vapor mixing ratio due to competition from the  $\text{CH}_2\text{OO} + (\text{H}_2\text{O})_n$  reaction (Figure E.3b). Hydroperoxy methylformate (HPMF), seemingly the sole product of the  $\text{CH}_2\text{OO} + \text{HCOOH}$  reaction (Figure E.11 in the Supporting Information), is observed only under very dry conditions in accordance with previous reports (Hasson *et al.*, 2001b; Neeb *et al.*, 1997). This is because formic acid in ozonolysis experiments is rarely present at the levels needed to compete with water vapor. In addition to compounds reported in Table E.1, RH-dependent yields of minor species like acetic acid were also observed ( $< 0.06$ ). Representative CIMS mass spectra showing all products are given in Figure E.12 in the Supporting Information. Acetic acid has not been identified in past isoprene ozonolysis studies, but serves as an important clue in deducing the fragmentation patterns of  $\text{C}_4$  Criegees.

HMHP is the most abundant  $\text{CH}_2\text{OO} + (\text{H}_2\text{O})_n$  product, followed by formic acid, then  $\text{H}_2\text{O}_2$  (+ HCHO). The maximum HMHP yield is determined to be  $\sim 44\%$  from isoprene ( $\sim 73\%$  from  $\text{CH}_2\text{OO}$ ), somewhat higher than other values reported in the literature. Insightful comparisons with literature values prove challenging, however, due to the poor agreement in  $\text{CH}_2\text{OO} + (\text{H}_2\text{O})_n$  product yields. For example, single-point "humid" HMHP and  $\text{H}_2\text{O}_2$  yields are reported to be 0.09–0.30 and 0.01–0.12, respectively (Becker *et al.*, 1990; Hasson *et al.*, 2001a; Neeb *et al.*, 1997; Sauer *et al.*,

1999; Simonaitis *et al.*, 1991). Some of the inconsistencies in past experiments have been attributed to the challenge of quantifying hydroperoxides with offline aqueous methods (*e.g.* high-performance liquid chromatography, HPLC).

Interestingly, we find HMHP yields decrease above RH  $\sim$ 40% (Figure E.3b). The reduction in yield for HMHP at high humidity is almost fully compensated by an increase in yield for HCOOH (Figure E.3d). Although wall-mediated reaction is a convenient explanation, our RH-dependent corrections for wall loss using authentic compounds should account for this chemistry (Figure E.10 in the Supporting Information). Instead, model simulation results in Section E.3.2 support the idea that the RH-dependent yields of HMHP and HCOOH are controlled by reactions of both the water monomer and dimer. The dimer becomes exceedingly more abundant at higher RH. As the model simulations fit concentration data that have been wall-loss corrected, the heterogeneous reaction is not included in the mechanism. The atmospherically-relevant reaction of water dimer with CH<sub>2</sub>OO was first suggested by Ryzhkov and Ariya (Ryzhkov and Ariya, 2003, 2004, 2006) and later confirmed by experimental works (Berndt *et al.*, 2014; Chao *et al.*, 2015). Ryzhkov and Ariya suggested the decomposition products to be H<sub>2</sub>O<sub>2</sub> and HCHO; however, our data are more consistent with HCOOH as the major product from this reaction.

Past studies explored a large range in water vapor mixing ratio (9000–20,000 ppm, RH  $\sim$  28–63% at 298 K) while reporting only a single 'humid' yield for products. Thus, it is possible that poor literature agreement may be due to snapshot observations along different humidity points in the HMHP yield curve. These disagreements are likely exacerbated by the absence of wall loss corrections, which depend on the reaction vessel. To our knowledge, only two other HMHP yield studies have been performed at multiple RH conditions (Hasson *et al.*, 2001a; Huang *et al.*, 2013). Hasson *et al.* (2001a) and Huang *et al.* (2013) did not report yield trends similar to this work, *i.e.*, their data reported a rise-to-maximum relationship of HMHP with RH (maximum yields of 16% and 25%, respectively). Yet, despite the fitting function used by Hasson *et al.* (2001a), their data show that the average HMHP yield at RH  $\sim$ 80% ( $\sim$ 0.12  $\pm$  0.03) is lower than its yield at RH  $\sim$ 40% ( $\sim$ 0.16  $\pm$  0.04) for isoprene – congruent with our observed trends.

We are unsure of the reasons for discrepancies with the Huang *et al.* (2013) work. In addition to the plateauing HMHP yield, Huang *et al.* (2013) reported a declining yield of HCOOH with humidity (*e.g.* 40% yield of HCOOH at RH 5% that decreases to 30% yield at RH 90%). It is difficult to understand how HCOOH can

be produced in higher yields under dry conditions when HCOOH formation from Criegee isomerization is minor compared to the major channel of  $\text{CH}_2\text{OO} + (\text{H}_2\text{O})_n$  (Herron and Huie, 1977; Su *et al.*, 1980). Again, given the lower HMHP yields reported by studies using offline analysis techniques, it is possible that aqueous losses may have occurred and direct comparisons are not possible. Furthermore, the bis-hydroxymethyl peroxide (BHMP) reported in Huang *et al.* (2013) (and absent in this work) may hint at side reactions that are symptomatic of the high reagent concentrations (ppm level) used in that work or condensed-phase chemistry of  $\text{H}_2\text{O}_2$  and HCHO.

### E.3.2 Toward a Unifying Mechanism

Major atmospheric models either do not represent ozonolysis chemistry or provide a significantly abridged version that generally neglects the formation of major compounds such as HMHP (Bey *et al.*, 2001; Saunders *et al.*, 2003). Here, we describe a detailed chemical mechanism based on the new data presented in this work and those available in the literature. The *in situ* observations of oxygenated volatile organic compounds and  $\text{HO}_x$  enable us to place new constraints on many aspects of the mechanism. Mechanism simulations of HCHO assumes that are no observational interferences from ROOH or other compounds, which is currently unverified for the LIF instrument used here but has been identified for proton-transfer-reaction (PTR-) and GC-based instruments (Rivera-Rios *et al.*, 2014). The proposed mechanism provides enough chemical specificity to capture the RH-dependent yields of OH, carbonyls (HCHO, MACR, MVK), and major products of  $\text{CH}_2\text{OO} + (\text{H}_2\text{O})_n$  chemistry. Although uncertainties persist along several channels in the ozonolysis chemistry, especially in the fate of the  $\text{C}_4$  Criegees, the proposed scheme is a good starting point for further development and use in atmospheric models.

#### E.3.2.1 POZ and $\text{C}_4$ Criegee Reactions

Figure E.4 shows the proposed reaction scheme for isoprene ozonolysis. Compounds observed in this work are shown in red. The chemical structures of some of the minor oxygenated species may not be unique, as this CIMS technique cannot distinguish isobaric species. We used the branching ratios for POZ formation that was suggested by Aschmann and Atkinson (Aschmann and Atkinson, 1994), which implies that the lower steric hindrance from the 3,4-addition of ozone is more important than the effect of the electron-donating  $\text{CH}_3$  group in the 1,2-addition (Zhang and Zhang, 2002). It is assumed that there is negligible conformational intercon-

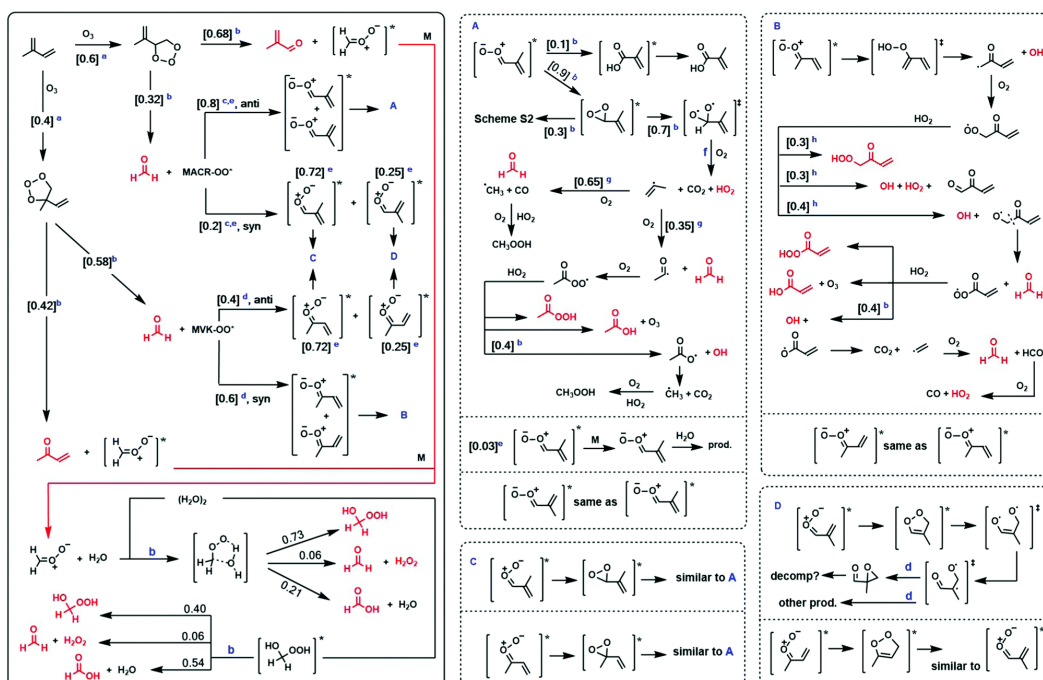


Figure E.4: Overall scheme of isoprene ozonolysis and reactions of Criegee intermediates, with proposed isomerization and decomposition pathways of  $C_4$  Criegees. Observed product species are shown in red. The reaction of  $CH_2OO$  with  $O_3$  and isoprene, although present in the model mechanism, are not shown in the figure. Literature values: [a] Aschmann and Atkinson (1994), [b] this work, [c] Zhang and Zhang (2002), [d] Kuwata and Valin (2008), [e] Kuwata *et al.* (2010), [f] Horie *et al.* (1994b) and Nguyen *et al.* (2009a,b), [g] Orlando *et al.* (1999), [h] Praske *et al.* (2015).

version between Criegees due to their zwitterionic character (Hull, 1978; Taatjes *et al.*, 2013), *i.e.*, the barrier to interconversion is expected to be large (Anglada *et al.*, 1996). We note that data available for Criegees with allylic groups, which would presumably facilitate interconversion, is still scarce. Thus, the assumptions and reaction channels discussed here may need to be re-evaluated in future work.

Evidence of bimolecular reactions of the  $C_4$  SCI is not significant. For example, the signals of  $C_4$   $\alpha$ -hydroxyalkyl hydroperoxides that are analogous to HMHP, *e.g.* from the reaction of *anti* MACROO +  $(H_2O)_n$ , were not observed here. Furthermore, MACR + MVK yields did not significantly increase following  $SO_2$  addition, *e.g.* as would be expected from the MACROO +  $SO_2 \rightarrow$  MACR +  $SO_3$  reaction. The insignificant production of MACR from the MACROO +  $SO_2$  reaction and the fast *anti*-SCI +  $H_2O$  rate coefficient determined recently ( $2.4 \times 10^{-14} \text{ cm}^3 \text{ molec}^{-1} \text{ s}^{-1}$ ) (Sheps *et al.*, 2014) favor the hypothesis that the stabilization fraction of the

C<sub>4</sub> Criegees is small, as opposed a larger population of SCI where bimolecular reactions are non-competitive. Thus, we assumed a Criegee stabilization fraction of 0.03 as suggested by Kuwata and Valin (2008). However, accessible unimolecular pathways of CIs and SCIs are often identical, so it is not possible for this study to fully distinguish the two fates. An SCI unimolecular rate constant of  $\sim 250 \text{ s}^{-1}$  would also be consistent with observations. The 0.03 "stabilization fraction" can be viewed as an effective fraction of Criegees that react bimolecularly under H<sub>2</sub>O-dominated conditions. Extensive C<sub>4</sub> Criegee decomposition (hot or thermalized) is consistent with the high yields (>80%) of HCHO that are observed in this work and elsewhere (Grosjean *et al.*, 1993b). The production of HCHO from the prompt POZ decomposition is constrained by MVK + MACR yields to be approximately  $\sim 40\%$  by mole with respect to isoprene loss. CH<sub>2</sub>OO is fully scavenged by water in most of our experiments, so little additional HCHO can originate from side reactions of CH<sub>2</sub>OO at atmospherically-relevant RH.

After the POZ decomposition, the distribution of the *syn/anti* conformers of the C<sub>4</sub> Criegees is thought to be asymmetric. We used the branching ratios suggested by Kuwata and coworkers (Kuwata *et al.*, 2010; Kuwata and Valin, 2008), with the caveat that the MVK-OO\* conformer distribution is loosely based on the hot acetaldehyde oxide, for lack of direct information. Unimolecular reactions of the C<sub>4</sub> Criegees have been suggested to occur *via* 5-member dioxole or 3-member dioxirane intermediates (Kuwata *et al.*, 2010; Kuwata and Valin, 2008; Vereecken *et al.*, 2012). The model mechanism allows C<sub>4</sub> Criegees that are *syn* and *anti* to vinyl groups to form dioxole and dioxirane intermediates, respectively, using the theoretically-predicted dioxole/dioxirane branching ratios (Kuwata and Valin, 2008). Dioxoles have been suggested to isomerize into products containing carbonyl and epoxide functional groups, which may further decompose (Kuwata *et al.*, 2010); however, the CIMS technique used in this work is likely not sensitive to these specific compounds. The dioxole products were not traced in the model because they represent an insignificant fraction of the carbon in the mechanism ( $\sim 3\%$ ) and are not thought to impact OH or HCHO yields. A minor fraction of the *anti* MACROO\* is allocated toward hot acid formation, yielding methacrylic acid (which may also occur *via* a dioxirane intermediate) (Cremer *et al.*, 1998). The dioxirane channels represent a larger fraction of the carbon in the ozonolysis. We followed the recommendations of Peeters, Vereecken, and coworkers (Nguyen *et al.*, 2009a,b), in conjunction with observations derived from acetaldehyde oxide (Horie *et al.*, 1994b), to assign the majority of the dioxirane fate to the decarboxylation pathway

(products  $\text{CO}_2 + \text{HO}_2 + \text{alkyl radical}$  for dioxiranes in the primary position). A decarboxylation branching ratio of  $\sim 0.7$  gave good agreement with observations. As these dioxiranes have allylic functionality, we assign the balance of the carbon to a proposed isomerization pathway (Figure E.13 in the Supporting Information) that may form a stable product. The alkyl radical that is produced in the decarboxylation step in Route A is the methylvinyl radical, which is known to generate  $\text{HCHO} + \text{peroxyacetyl radical}$  ( $\sim 0.35$ ) or  $\text{HCHO} + \text{methylperoxyl radical} + \text{CO}$  ( $\sim 0.65$ ) in the presence of oxygen (Orlando *et al.*, 1999). It is probable that the observed acetic acid (0.02–0.06 from dry to humid) is produced from the reaction of peroxyacetyl radicals with  $\text{HO}_2$  or  $\text{RO}_2$  (Crawford *et al.*, 1999; Hasson *et al.*, 2004; Horie and Moortgat, 1992; Madronich and Calvert, 1990). We speculate that the higher acetic acid yield under more humid conditions may be due to unidentified wall reactions. The methylperoxyl radical is a precursor to methyl hydroperoxide under  $\text{HO}_2$ -dominant conditions. Methyl hydroperoxide has been identified in previous works (Gäb *et al.*, 1995; Sauer *et al.*, 1999), but without complete mechanistic knowledge of its chemical source.

The *syn* MVKOO\* will decompose to OH and a  $\beta$ -oxy alkyl radical *via* a vinylhydroperoxide intermediate (B route). The further reactions of the  $\beta$ -oxy alkylperoxyl radical ( $\text{RO}_2$ ) are much more uncertain. In the mechanism suggested here, this chemistry is proposed to proceed similarly to the  $\text{RO}_2$  radicals found in MVK + OH chemistry that have analogous functionality (Praske *et al.*, 2015). We followed the recommendations in Praske *et al.* (2015) for the branching ratios of the three product channels with  $\text{HO}_2$ :  $\beta$ -oxy hydroperoxide, 1,2-dicarbonyl + OH +  $\text{HO}_2$ , and alkoxy radical (RO) + OH +  $\text{O}_2$ . The RO radical fragments to formaldehyde and an acyl radical and promptly reacts with  $\text{O}_2$  to produce an acylperoxyl ( $\text{RC(O)OO}$ ) radical. The acylperoxyl radical may undergo three fates upon reaction with  $\text{HO}_2$  (Figure E.4B), modeled after reactions of peroxyacetyl (Moortgat *et al.*, 1989; Tomas *et al.*, 2001). These data suggest that decarboxylation is an important fate for this particular acylperoxyl radical, which affects both OH and formaldehyde in the process (*via* the chemistry of the vinyl radical) (Knyazev and Slagle, 1995).

### E.3.2.2 C<sub>1</sub> Criegee + Water Reaction

The mechanism illustrated in Figure E.4 was integrated into a kinetic model. Most of the rates and branching ratios available in the literature were imported for use in the model mechanism and assumed to be accurate. The product yields and rate

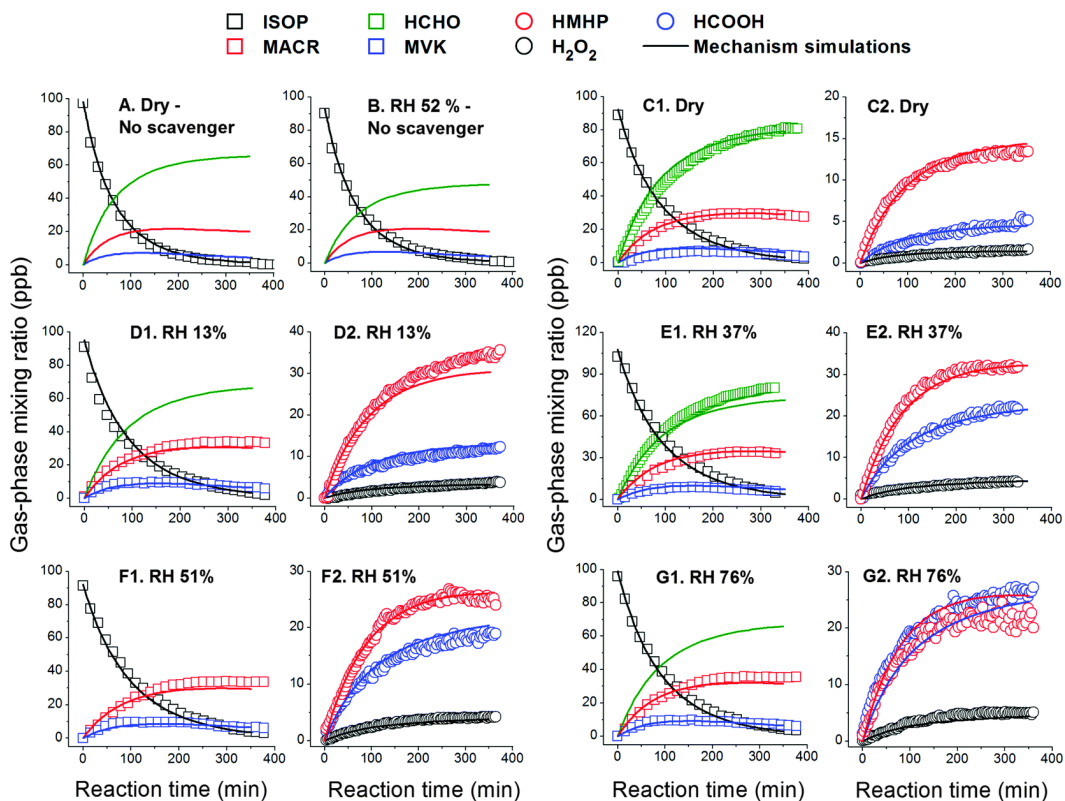


Figure E.5: Panels A–G show the comparison between gas-phase observations from different experiments (various markers) and results from model mechanism simulations based on Figure E.4 (solid lines). Subpanels show the mixing ratios of (1) isoprene and carbonyls and (2)  $\text{CH}_2\text{OO} + (\text{H}_2\text{O})_n$  products, when applicable. Simulations under "Dry" conditions used  $\text{RH} = 1.2\%$ . The displayed mixing ratios of HMHP and HCOOH have been corrected for first-order wall loss (Figure E.10 in the Supporting Information). The model inputs are shown in the Supporting Information. Experimental conditions for the measured data are found in Table E.1.

coefficients of Criegee reactions labeled [b] in Figure E.4 were empirically tuned to provide satisfactory agreement with observational data within the full RH range, as shown in Figure E.5. The reaction inputs into the kinetic model are shown in the Supporting Information. We find that variations in the molar yields of HMHP, HCOOH, HCHO and  $\text{H}_2\text{O}_2$  with RH can only be simulated if the reaction with water dimer is included in the mechanism. The mixing ratio of water dimers was calculated based on their equilibrium thermodynamics at 295 K (Figure E.14 in the Supporting Information) (Owicky *et al.*, 1975).

Some of the observed  $\text{H}_2\text{O}_2$  in the ozonolysis experiments (Table E.1) originates from the  $\text{HO}_2 + \text{HO}_2 \rightarrow \text{H}_2\text{O}_2 + \text{O}_2$  reaction (Figure E.15 in the Supporting Information). Using published rate constants and  $\text{HO}_2$  observations we estimate the

HO<sub>2</sub> self-reaction accounts for ~50% of the observed H<sub>2</sub>O<sub>2</sub>. However, considering the uncertainties in the HO<sub>2</sub> and H<sub>2</sub>O<sub>2</sub> observations we cannot exclude the possibility that the HO<sub>2</sub> self-reaction explains the entirety of the observed H<sub>2</sub>O<sub>2</sub>, and thus, that the CH<sub>2</sub>OO + (H<sub>2</sub>O)<sub>n</sub> → H<sub>2</sub>O<sub>2</sub> + HCHO channel has zero yield (see error bounds in Figure E.15 in the Supporting Information). We adjusted the product branching ratios for the CH<sub>2</sub>OO + (H<sub>2</sub>O)<sub>n</sub> reactions to remove the average contribution from HO<sub>x</sub> chemistry, and this is shown in the left-most panel of Figure E.4. The product branching in the dimer reaction favors formic acid formation over HMHP formation, which is consistent with the suggestion that the reaction of CH<sub>2</sub>OO with water dimer to form HMHP is exothermic, and some of the excited HMHP produced by that pathway may further decompose (in this case to formic acid + H<sub>2</sub>O) with water acting as a catalyst (Ryzhkov and Ariya, 2004).

We used the following rate coefficients for the reaction of CH<sub>2</sub>OO with water in the model mechanism:  $k_{H_2O} = 9 \times 10^{-16} \text{ cm}^3 \text{ molec}^{-1} \text{ s}^{-1}$  and  $k_{(H_2O)_2} = 8 \times 10^{-13} \text{ cm}^3 \text{ molec}^{-1} \text{ s}^{-1}$ . The water monomer reaction rate coefficient falls within the upper limit determined by Welz *et al.* (2012) and by other works ( $<4 \times 10^{-15} \text{ cm}^3 \text{ molec}^{-1} \text{ s}^{-1}$ ). The dry (RH ~1%) observations provided constraints for the monomer rate coefficient, and the dimer rate coefficient was adjusted until model results satisfactorily reproduces measurements. We found that a dimer reaction coefficient faster than that of the monomer reaction, but slower than the coefficient suggested by some studies ( $4\text{--}6.5 \times 10^{-12} \text{ cm}^3 \text{ molec}^{-1} \text{ s}^{-1}$ ; Berndt *et al.*, 2014; Chao *et al.*, 2015; Lewis *et al.*, 2015), gave the best fit with the observational results across all RH conditions.

Figure E.16 in the Supporting Information shows results of a sensitivity study of the water rate coefficients in the model, which concludes that the rate coefficient of Chao *et al.* (2015) is too large to simulate the data in this work. Our suggested dimer rate coefficient of  $k_{(H_2O)_2} = 8 \times 10^{-13} \text{ cm}^3 \text{ molecule}^{-1} \text{ s}^{-1}$  is consistent with those of Newland *et al.* (2015), who found that  $5.6 (\pm 7.0) \times 10^{-13} \text{ cm}^3 \text{ molec}^{-1} \text{ s}^{-1}$  best describe their chamber data. Leather *et al.* (2012) also found the rate coefficient of CH<sub>2</sub>OO with "water" to be in the range of  $\sim 1 \times 10^{-15} - 1 \times 10^{-12} \text{ cm}^3 \text{ molec}^{-1} \text{ s}^{-1}$  when measuring HCOOH. HCOOH is the product of both the water monomer and dimer reaction with CH<sub>2</sub>OO, so the observed range is in agreement with this work. The difference between reported CH<sub>2</sub>OO + water dimer rate coefficients in the literature is striking, but the source of the disagreement is unclear.

The reaction timescales, Criegee generation methods, reaction vessel character-

istics, and Criegee concentrations in literature works are different – all of which may play a role in the discrepancy. Furthermore, if water vapor may intercept the hot Criegee directly during ozonolysis reactions, in a manner analogous to the interception of excited alkyl radicals by O<sub>2</sub> (Glowacki *et al.*, 2012), then there may be significant deviations between chamber and direct kinetic determinations as direct determinations produce and investigate SCI preferentially. The result is a promotion of the H<sub>2</sub>O reaction over the (H<sub>2</sub>O)<sub>2</sub> reaction during ozonolysis. Assuming CI interception occurs to a non-negligible extent, observations from chamber studies would be more immediately relevant for atmospheric modeling than current data from direct determinations.

Figure E.14c in the Supporting Information shows the relative contribution of each reaction using the aforementioned rate coefficients, where the dimer reaction can contribute up to ~65% as the humidity approaches 100%. However, the water monomer reaction is an important sink for CH<sub>2</sub>OO under all atmospherically-relevant RH.

### E.3.2.3 OH and HO<sub>2</sub> formation

The production of OH can be visualized from the decay of isoprene in the experiments where an OH scavenger was not present (Figure E.5 a and b). OH was directly measured by LIF; however, the high dilution ratio used in the laboratory to conserve chamber volume degraded the signal-to-noise of the instrument. In addition, the experimental conditions in the reaction (including high peroxide mixing ratios) and unknown interferences that may be related to unsaturated hydrocarbon + ozone chemistry resulted in uncertainty bounds in the direct OH determination that were too high to constrain yields (Mao *et al.*, 2012; Nguyen *et al.*, 2014b). Thus, a combination of modeling and isoprene decay measurements was used to estimate [OH]. Estimations of OH sources in the model mechanism relied on constraints provided by other products. An overall OH yield of approximately 28(±5)% gives good agreement with observations under both dry and humid conditions, *e.g.* the comparison between observed and simulated isoprene decays produced least-squares slope = 1.023, R<sup>2</sup> = 0.999 at RH < 4% and slope = 1.015, R<sup>2</sup> = 0.998 at RH 52%, and is consistent with the recommended value by IUPAC (25%) (Atkinson *et al.*, 2006). It should be noted that not all of this OH is produced from the prompt VHP channel. This would necessitate almost 100% *syn* branching for MVKOO\* and for the following radical chemistry to be OH neutral. Instead, the constraints placed by

closed-shell products in the mechanism predict that prompt decomposition (from *syn*-MVKOO\*) accounts for a 14% yield of OH, with respect to the reaction of isoprene, and further chemistry of the  $\beta$ -oxy alkyl radical generates another 12%. The remaining minor fraction arises from unimolecular reactions of the C<sub>4</sub> Criegees. Neither the POZ decomposition nor the following RO<sub>2</sub> chemistry is expected to be sensitive to water vapor, in good agreement with the stable OH yields between dry and humid conditions. Our OH source contribution results are fairly consistent with those using a statistical-dynamical master equation and transition state theory, which predicts an OH prompt production yield of 11% for a total yield of 25% (Zhang and Zhang, 2002).

HO<sub>2</sub> is generated and consumed along various reaction channels in ozonolysis (Figure E.4). The HO<sub>x</sub> cycling of OH and HO<sub>2</sub> also occurs in conjunction with ozonolysis in the model mechanism (Supporting Information). Major sources of HO<sub>2</sub> from ozonolysis include decarboxylation of primary dioxiranes (Route A) and the further chemistry of the  $\beta$ -oxy alkyl radical (Route B). A major sink of HO<sub>2</sub> in this work is the reaction with the RO<sub>2</sub> radical produced from cyclohexane (OH scavenger). As a result, the usage of other OH scavengers may change the HO<sub>2</sub> concentrations during similar experiments. Figure E.17 in the Supporting Information shows that HO<sub>2</sub> simulated using the kinetic model shown in the Supporting Information agrees fairly well with the measured values under dry and humid conditions at the start of the reaction (~40 ppt). As the reaction progresses, however, the agreement worsens (simulated HO<sub>2</sub> is lower than measured.) We believe this is because the simulated scheme does not trace second generation products, which appear to produce a significant quantity of HO<sub>2</sub>.

#### E.3.2.4 HCHO Formation

The difference in observed HCHO between the dry (RH ~1% in the simulation) and RH 37% experiments provides unique insights into the bimolecular reaction of CH<sub>2</sub>OO (Figure E.5, Panels c1 and e1). The model predicts that a non-negligible fraction of HCHO can be produced from the CH<sub>2</sub>OO reaction with ozone (Kjaergaard *et al.*, 2013; Wei *et al.*, 2014), the second most abundant reaction partner for CH<sub>2</sub>OO in our experiments, when the reaction conditions are dry. For  $k_{\text{CH}_2\text{OO}+\text{O}_3} \sim 1 \times 10^{-12} \text{ cm}^3 \text{ molec}^{-1} \text{ s}^{-1}$ , as has been previously suggested (Vereecken *et al.*, 2014), the best fit with observations is achieved by assuming a formaldehyde yield of 0.7 (while conserving a faster rate), instead of the recommended value of 1. While

it is possible that unknown pathways for the  $\text{CH}_2\text{OO} + \text{O}_3$  reaction exist, we believe it more likely that the model mechanism is missing a Criegee sink that is  $\sim 30\%$  of the effective  $\text{CH}_2\text{OO} + \text{O}_3$  reaction, but does not produce HCHO, when the reaction is performed dry. If a missing sink exists, it is not the Criegee self-reaction, as including even the fastest experimentally-determined rate coefficient did not alter the simulations (Su *et al.*, 2014). All side reactions of  $\text{CH}_2\text{OO}$  become negligible when RH reaches atmospherically relevant levels. Of the HCHO sources discussed in this work that are important under atmospherically relevant conditions, the initial POZ decomposition comprises the majority production pathway ( $\sim 60\%$ ). The model simulations predict that unimolecular reactions of  $\text{C}_4$  Criegees to contribute another relative  $\sim 35\%$  and the reaction of  $\text{CH}_2\text{OO} + (\text{H}_2\text{O})_n$  is a relatively small ( $\sim 5\%$ ) source of formaldehyde. As we noted above, the yield of HCHO and  $\text{H}_2\text{O}_2$  from this channel could be zero within uncertainties.

### E.3.2.5 Other Reactions of the $\text{C}_1$ Criegee

Finally, we use the  $\text{RO}_2 + \text{CH}_2\text{OO}$  rate coefficient of Vereecken *et al.* (2012) ( $k \sim 5 \times 10^{-12} \text{ cm}^3 \text{ molec}^{-1} \text{ s}^{-1}$ ) and the OH reaction kinetics for cyclohexane (Atkinson *et al.*, 2006) to examine whether the 50 ppm of OH scrubber produces enough  $\text{RO}_2$  to impact  $\text{CH}_2\text{OO}$  yields in the ozonolysis reaction. The model results suggest that cyclohexane  $\text{RO}_2$  radicals were not competitive with water as a Criegee scavenger during the experiments in this work. In addition, inserting the reaction of isoprene +  $\text{CH}_2\text{OO}$  into the model mechanism ( $k = 1.78 \times 10^{-13} \text{ cm}^3 \text{ molec}^{-1} \text{ s}^{-1}$ ), as suggested by Vereecken *et al.* (2014), did not significantly perturb the model simulation results. However, in studies where initial isoprene and ozone are present at ppm levels, the  $\text{CH}_2\text{OO} + \text{alkene}$  reaction may play a bigger role. These newly-identified reactions may be one source of discrepancy in literature yield data, underscoring the importance of using atmospherically-relevant mixing ratios of reactants or verifying that secondary chemistry is not affecting laboratory results.

### E.3.3 Competitive Rates of $\text{CH}_2\text{OO} + (\text{H}_2\text{O})_n$ and $\text{CH}_2\text{OO} + \text{SO}_2$

Although water reactions are thought to dominate the fate of  $\text{CH}_2\text{OO}$  in the atmosphere (Berndt *et al.*, 2014; Chao *et al.*, 2015; Fenske *et al.*, 2000; Newland *et al.*, 2015; Ryzhkov and Ariya, 2004), it has been suggested that the reaction of SCI with  $\text{SO}_2$  may be important from the perspective of  $\text{H}_2\text{SO}_4$  production and, thus, particle formation (Mauldin *et al.*, 2012). Here, we measure the competitive

rates of the reaction of isoprene SCIs with H<sub>2</sub>O and SO<sub>2</sub>, using isoprene mixing ratios that approach atmospheric levels (~20 ppb) and realistic concentrations of SO<sub>2</sub>. This measurement is sensitive to the combined effects of CH<sub>2</sub>OO and the C<sub>4</sub> SCIs of isoprene. However, it is clear that the dominant fraction of the bimolecular reactivity originates from CH<sub>2</sub>OO, illustrated by the similar SCI yields when using SO<sub>2</sub> as a scavenger compared to H<sub>2</sub>O (Table E.1). Notably, the orders of magnitude uncertainties that exist in the absolute rate coefficients for CH<sub>2</sub>OO bimolecular reactions become immaterial when determining relative rates (Anglada *et al.*, 2011; Atkinson and Lloyd, 1984; Herron *et al.*, 1982; Kurtén *et al.*, 2011; Kuwata and Valin, 2008; Ryzhkov and Ariya, 2004; Stone *et al.*, 2014; Welz *et al.*, 2012).

Figure E.6 shows the reaction progress for three relative rate experiments between H<sub>2</sub>O and SO<sub>2</sub> during an isoprene ozonolysis performed with an OH scavenger. At 15 ppb of SO<sub>2</sub> and 20% RH, representative of a dry and polluted day, greater than 90% of CH<sub>2</sub>OO reacted with water as evidenced by the large abundance of HMHP and HCOOH as compared to H<sub>2</sub>SO<sub>4</sub> (Figure E.6a). Only under the driest conditions (RH < 4%) does CH<sub>2</sub>OO appreciably oxidize SO<sub>2</sub> at initial levels of ~15 ppb (Figure E.6b). Although under these conditions, the water reaction is still the major reaction pathway for CH<sub>2</sub>OO. Here, we start to witness decreasing mixing ratios of HMHP with time, which is due to heterogeneous loss on acidic surfaces from the H<sub>2</sub>SO<sub>4</sub> production and is uncorrected in Figure E.6. Only under exceptionally dry (RH < 4%) and exceptionally high [SO<sub>2</sub>]<sub>0</sub> (~75 ppb) conditions does SO<sub>2</sub> oxidation become the dominant fate of CH<sub>2</sub>OO (Figure E.6c), although these specific conditions are rarely found on Earth.

The relative rate of  $k_{SO_2}/k_{(H_2O)_n} = 2.2 (\pm 0.3) \times 10^4$  determined from the data is in good agreement with the  $k_{SO_2}/k_{(H_2O)_n}$  range of  $(1-3) \times 10^4$  reported in other studies (Atkinson and Lloyd, 1984; Newland *et al.*, 2015; Welz *et al.*, 2012). However, these results are considerably different than those of Stone *et al.* (2014), who measured a lower limit of  $k_{SO_2}/k_{(H_2O)_n} > 4 \times 10^5$ . Although the source of the discrepancy is not clear, the experiments of Stone *et al.* (2014) were performed differently compared to this work. Stone *et al.* (2014) quantified CH<sub>2</sub>OO decay *via* chemical scavenging to form HCHO and made the assumption that HCHO production is proportional to CH<sub>2</sub>I (Criegee precursor) concentrations. Like other studies that measure CH<sub>2</sub>OO decay (Taatjes *et al.*, 2008), Stone *et al.* (2014) provides lower limits on  $k_{SO_2}/k_{(H_2O)_n}$  due to unknown processes that affect the first-order SCI decay when H<sub>2</sub>O is added. As this work captures at least one co-product of each branch in the CH<sub>2</sub>OO + (H<sub>2</sub>O)<sub>n</sub>

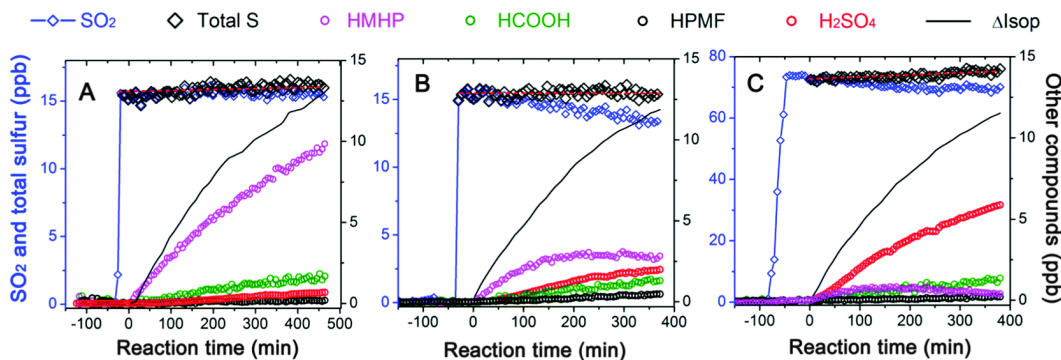


Figure E.6: Relative rate experiments of  $\text{H}_2\text{O}$  and  $\text{SO}_2$  as scavengers for  $\text{CH}_2\text{OO}$ , produced by the ozonolysis of  $\sim 20$  ppbv of isoprene at 298 K, under the following conditions: (A) 15 ppbv of  $\text{SO}_2$  and 20% RH, (B) 15 ppbv of  $\text{SO}_2$  and  $<4\%$  RH, and (C) 75 ppbv of  $\text{SO}_2$  and  $<4\%$  RH. Total sulfur (black diamonds) represents the sum of  $\text{SO}_2$  and  $\text{H}_2\text{SO}_4$ .

reaction, our measurement can be considered absolute. However, it must be noted that challenges in quantifying low  $[\text{H}_2\text{O}]$  and complex reaction products also give rise to significant uncertainties in this work – a limitation that likely permeates all studies of  $\text{SCI} + (\text{H}_2\text{O})_n$  reactions.

### E.3.4 Fates of $\text{CH}_2\text{OO}$ in the Atmosphere: A Case Study from SOAS

To put the competition between the reaction of  $\text{H}_2\text{O}$  and  $\text{SO}_2$  with  $\text{CH}_2\text{OO}$  into perspective, it would require 500 ppb of  $\text{SO}_2$  to have equal reactivity with  $\text{H}_2\text{O}$  at an average RH of 30% ( $T = 295$  K,  $P = 1$  atm). Many areas of the world are more humid than this RH level, especially in forested areas where biogenic emissions are high. At  $\text{RH} > 50\%$ , the amount of  $\text{SO}_2$  needed for equal reactivity would be found only in a power plant or volcanic plume. Here, we examine the fates of  $\text{CH}_2\text{OO}$  and molecular contributors to  $\text{SO}_2$  oxidation in a typical Southeastern United States forest that emits predominantly isoprene during summer. The comprehensive datasets were obtained by multiple investigators as part of the Southern Oxidant and Aerosol Study in Brent, AL during June of 2013 (<https://SOAS2013.rutgers.edu/>). A time-of-flight  $\text{CF}_3\text{O}^-$  CIMS provided measurements of  $\text{SO}_2$ ,  $\text{H}_2\text{O}_2$ , and oxidized organic compounds and a commercial weather station (Coastal Environmental Systems model Zeno 3200) provided measurements of T, P, and RH needed to calculate water vapor mixing ratio. The measurement site was occasionally impacted by  $\text{SO}_2$  pollution from nearby power plants.

Figure E.7 shows the measured  $\text{CH}_2\text{OO} + (\text{H}_2\text{O})_n$  products and the  $\text{CH}_2\text{OO} +$

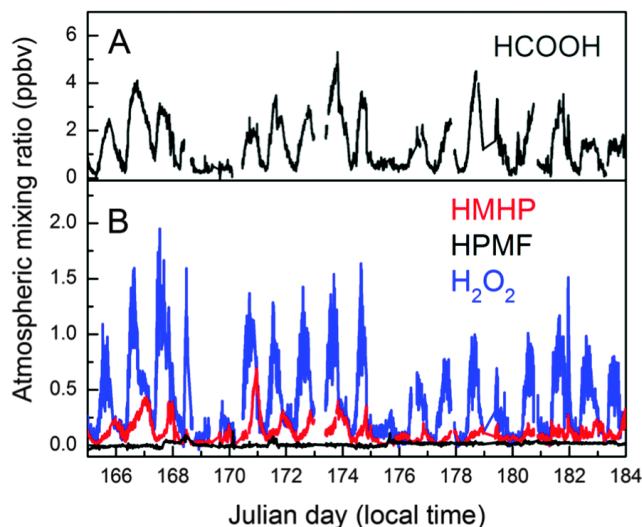


Figure E.7: Measurements of compounds that are formed *via*  $\text{CH}_2\text{OO}$  bimolecular reactions during the SOAS 2013 campaign (A) formic acid, and (B) HMHP, HPMF, and  $\text{H}_2\text{O}_2$ .  $\text{HCOOH}$  and  $\text{H}_2\text{O}_2$ , in particular, have multiple photochemical sources.

$\text{HCOOH}$  product for the duration of the SOAS study. While  $\text{HCOOH}$  and  $\text{H}_2\text{O}_2$ , two compounds with multiple photochemical sources, are known to have high concentrations at the Earth's surface, the presence of large abundances of HMHP produced from biogenic ozonolysis chemistry has previously not been fully appreciated. The mixing ratio of HMHP reaches 600 ppt during some events at this site (Figure E.7b). Other limited observations of HMHP report even higher mixing ratios (Lee *et al.*, 1993a). Concentrations of HMHP are comparable to the sum of two major products of the isoprene + OH oxidation under  $\text{HO}_2$ -dominated conditions (ISOPOOH + IEPOX) during the SOAS campaign (Nguyen *et al.*, 2015a). We note, however, that the interpretation of the ambient surface mixing ratio of HMHP is challenging as it is affected by poorly-constrained oxidative and photolytic loss processes. Additionally, the nocturnal peak concentrations of HMHP reflect both chemical production and nighttime boundary layer dynamics.

The persistently humid (2–3 vol%  $\text{H}_2\text{O}$ ) and occasionally polluted atmosphere at SOAS provides a useful case study to examine the reactions of  $\text{CH}_2\text{OO}$  (Figure E.18 in the Supporting Information). Despite plumes that approached 10 ppb,  $\text{SO}_2$  only negligibly impacted the  $\text{CH}_2\text{OO}$  fate. Using laboratory-derived relative rate results (Section E.3.3),  $\text{CH}_2\text{OO}$  loss in the gas phase was almost entirely controlled by the  $\text{H}_2\text{O}$  reactions (>98%) for every day of the SOAS study (Figure E.19a in the Supporting Information). At peak  $\text{SO}_2$  mixing ratios, the fraction of  $\text{CH}_2\text{OO}$

that was oxidized by SO<sub>2</sub> was below 1%. In comparison, the effective reaction with HCOOH is slightly more efficient at 1–2% of the total CH<sub>2</sub>OO fate due to high HCOOH mixing ratios (~4 ppb, Figure E.7a) and a faster rate coefficient ( $k_{\text{HCOOH}}/k_{\text{SO}_2} \sim 2.8$ ; Sipilä *et al.*, 2014). Still, the product of the CH<sub>2</sub>OO + HCOOH reaction, HPMF, was not present at quantifiable concentrations during the majority of the month-long study (Figure E.7b). Using peak SO<sub>2</sub> and HCOOH mixing ratios observed during the SOAS campaign, we find that the water reaction is dominant at all atmospherically-relevant RH (Figure E.19b in the Supporting Information).

Given the ubiquity of water in the troposphere, it is more informative to explore the CH<sub>2</sub>OO reactions from the point of view of SO<sub>2</sub> and HCOOH oxidation. We use the observed mixing ratios of ozone, abundant exocyclic alkenes (isoprene and  $\beta$ -pinene), and water vapor to estimate the steady-state concentrations of CH<sub>2</sub>OO at this site ( $\sim 2 \times 10^3$  molec cm<sup>3</sup> in the daytime) for the month-long study (Figure E.17 in the Supporting Information). The production term was calculated from the ozonolysis reaction, using respective SCI yields of 0.6 for isoprene (this work) and 0.3 for  $\beta$ -pinene (assuming that the scavenged SCI are mostly CH<sub>2</sub>OO; Hasson *et al.*, 2001a). The loss term assumes H<sub>2</sub>O and (H<sub>2</sub>O)<sub>2</sub> are the only sinks for CH<sub>2</sub>OO at this site (Figure E.19b in the Supporting Information).  $\alpha$ -Pinene is the second most abundant alkene in this forest but its ozonolysis is not thought to produce CH<sub>2</sub>OO. The rate coefficients of relevant reactions (Atkinson *et al.*, 2006; Khamaganov and Hites, 2001) were calculated using measured temperature inputs (292–306 K) during SOAS:  $k_{\text{ISO}+\text{O}_3}$  ( $\sim 1 \times 10^{-17}$  cm<sup>3</sup> molec<sup>-1</sup> s<sup>-1</sup>),  $k_{\beta\text{-PIN}+\text{O}_3}$  ( $\sim 2 \times 10^{-17}$  cm<sup>3</sup> molec<sup>-1</sup> s<sup>-1</sup>),  $k_{\text{OH}+\text{SO}_2}$  ( $\sim 1 \times 10^{-12}$  cm<sup>3</sup> molec<sup>-1</sup> s<sup>-1</sup>), and  $k_{\text{OH}+\text{HCOOH}}$  ( $\sim 4.5 \times 10^{-13}$  cm<sup>3</sup> molec<sup>-1</sup> s<sup>-1</sup>). The average OH concentration used in the calculation was  $1 \times 10^6$  molec cm<sup>-3</sup>. For CH<sub>2</sub>OO reaction coefficients, we used  $k_{\text{SO}_2}/k_{(\text{H}_2\text{O})_n} \sim 2.2 \times 10^4$  (where  $n = 1, 2$ ; this work), absolute rate coefficients as reported in Section E.3.2.2, and two different relative rate determinations for HCOOH reactions that are notably different:  $k_{\text{HCOOH}}/k_{\text{SO}_2} \sim 2.8$  (" $k_{\text{HCOOH1}}$ ", Sipilä *et al.* (2014)) and  $k_{\text{HCOOH}}/k_{(\text{H}_2\text{O})} \sim 1.4 \times 10^4$  (" $k_{\text{HCOOH2}}$ ", Neeb *et al.* (1997)). Using  $k_{\text{SO}_2}/k_{(\text{H}_2\text{O})_n}$  and  $k_{(\text{H}_2\text{O})}$  in this work,  $k_{\text{HCOOH1}} \approx 5.5 \times 10^{-11}$  cm<sup>3</sup> molec<sup>-1</sup> s<sup>-1</sup> and  $k_{\text{HCOOH2}} \approx 2.0 \times 10^{-11}$  cm<sup>3</sup> molec<sup>-1</sup> s<sup>-1</sup>.

Figure E.8a shows that CH<sub>2</sub>OO accounts for <6% of the gas-phase SO<sub>2</sub> oxidation at the SOAS site. This is in stark contrast to the proposed 50% contribution of "compound X" (suggested to be related to Criegee chemistry) to the oxidation of SO<sub>2</sub> in a Finnish boreal forest (Mauldin *et al.*, 2012). The discrepancy has

been suggested to be due to the different distribution of volatile alkenes in boreal forests, *i.e.*, that the SCI from  $\alpha$ -pinene may have a higher relative contribution to SO<sub>2</sub> oxidation. However, given the large OH yields from  $\alpha$ -pinene ozonolysis (0.70–0.91) (Atkinson and Aschmann, 1993; Chew and Atkinson, 1996; Paulson *et al.*, 1998; Rickard *et al.*, 1999; Siese *et al.*, 2001), and the fast decomposition rates of larger Criegees (this work and elsewhere), the population of SCIs that are available for bimolecular reaction from  $\alpha$ -pinene is expected to be small and their contribution to sulfate formation, thus, an open question. In cleaner environments, a significant pathway toward new particle formation may be the production of extremely low volatility compounds from  $\alpha$ -pinene ozonolysis (Ehn *et al.*, 2014; Jokinen *et al.*, 2014), through the VHP channel and subsequent autoxidation reactions (Crouse *et al.*, 2012) of the RO<sub>2</sub>. In comparison, CH<sub>2</sub>OO may oxidize a larger amount (<35%) of HCOOH, as its CH<sub>2</sub>OO reaction is faster and its OH reaction is slower than the analogous reactions for SO<sub>2</sub>. However, depositional losses, instead of oxidation, is thought to dominate the atmospheric fate of HCOOH ( $\tau_{dep} \sim 20\text{--}40$  h (at 1.5 km PBL height),  $\tau_{OH} \sim 620$  h,  $\tau_{SCI} \sim 1800$  h) (Nguyen *et al.*, 2015a). Finally, we conclude that CH<sub>2</sub>OO does not significantly affect the atmospheric lifetime of SO<sub>2</sub> or HCOOH.

#### E.4 Atmospheric Implications

This work provides new insights into the reactions of isoprene-derived Criegee intermediates, especially for the decomposition pathways of the excited C<sub>4</sub> Criegees where scarce experimental data are available. The model mechanism in this work suggests that C<sub>4</sub> Criegees decompose to OH, HCHO, and other products in the atmosphere without significantly producing SCI that participate in bimolecular reactions. Some existing atmospheric models, such as the Master Chemical Mechanism (MCM), assume the C<sub>4</sub> Criegees lose O(<sup>3</sup>P) to form MVK and MACR, although this is not supported by our observations. A significant portion of the OH and HCHO yields is secondary. One reaction, subset CH<sub>2</sub>OO + (H<sub>2</sub>O)<sub>*n*</sub>, accounts for almost all of the SCI bimolecular reactions in isoprene ozonolysis under typical atmospheric conditions. This implies that isoprene-derived SCIs are a negligible contributor to H<sub>2</sub>SO<sub>4</sub> production in the atmosphere. If stabilized Criegees indeed play a role in new particle formation, the events will be localized to regions that are not dominated by the reactivity of ozone with isoprene. Those areas may instead be abundant in the small hydroperoxides that are quickly deposited to plant canopies (Nguyen *et al.*, 2015a). Our data are consistent with the suggestion that isoprene emissions

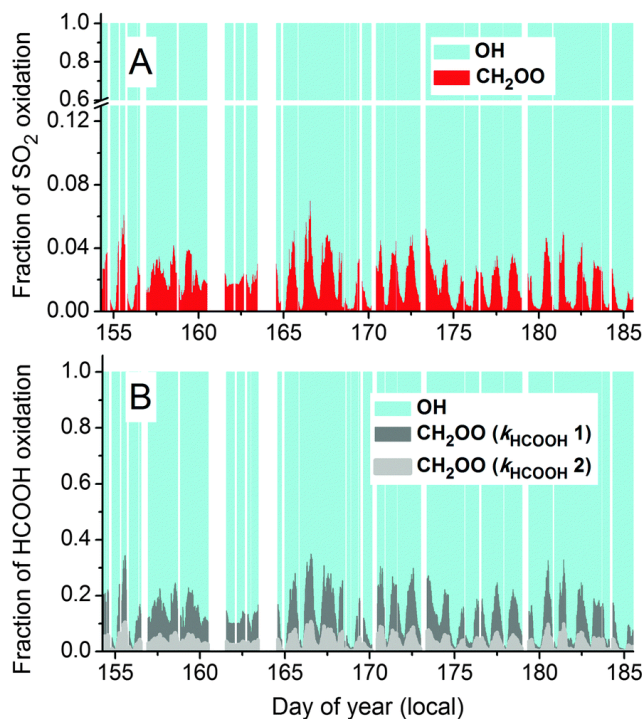


Figure E.8: Significance of CH<sub>2</sub>OO as an oxidant for (A) SO<sub>2</sub> and (B) HCOOH. In panel B, relative rate determinations by (1) Sipilä *et al.* (2014) and (2) Neeb *et al.* (1997) were used.

can suppress new particle formation (Kiendler-Scharr *et al.*, 2009), although the specific inhibition mechanism is still unclear, while these events readily occur in boreal forests (Mäkelä *et al.*, 1997). Discussions of whether monoterpene SCI in Boreal forests may appreciably oxidize SO<sub>2</sub> will hinge on the understanding of their unimolecular lifetimes and (H<sub>2</sub>O)<sub>*n*</sub> reactivity. Lastly, due to the structurally-specific reactivities of SCI, model simulations of ozonolysis chemistry should explicitly speciate alkenes and incorporate a conformationally-dependent reaction scheme. Incorporation of the isoprene ozonolysis mechanism (Figure E.4 and Supporting Information) into atmospheric models will likely improve the accuracy of OH, HO<sub>2</sub>, and trace gas simulations in the atmosphere.

## E.5 Supporting Information

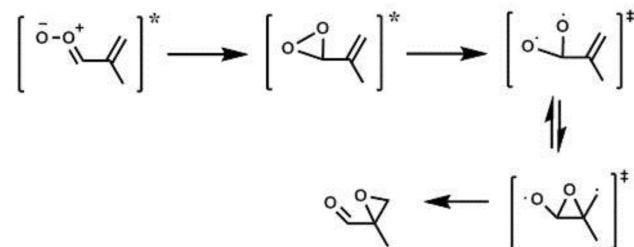


Figure E.9: (A) Partial calibration of the humidity dependence of HMHP ion sensitivity in CIMS. The  $\text{HO}_2 + \text{HCHO}$  reaction (from the photolysis of 4ppmv of formaldehyde, yellow shaded region) was used to produce approximately 5.7 ppbv of HMHP in the atmospheric chamber at 298K and 1 atm. The HMHP mixing ratio was allowed to stabilize for 1 hour before water-dependent calibration started. The stabilized HMHP mixing ratio from the chamber was sampled in the dark by CIMS, with nitrogen dilution streams that contained various mixing ratios of water: Gray regions denote 147 sccm of chamber air (dry) mixed with 1600 sccm of a dry ( $[\text{H}_2\text{O}] < 100$  ppmv) nitrogen flow (similar to standard operation), blue regions denote 147 sccm of chamber air mixed with 1600 sccm of a humid ( $[\text{H}_2\text{O}]$  up to 4000 ppmv) nitrogen flow, and white regions denote a break in sampling or sampling of 147 sccm of clean air mixed with 1600 sccm of a dry nitrogen flow. Data from the gray regions were used to confirm that the mixing ratio of HMHP in the chamber did not change significantly throughout the calibration period. Data from the white regions were used to confirm that the background (free of HMHP) did not shift throughout the calibration period. (B) The complete relationship of CIMS ion sensitivity vs. water vapor in the CIMS flow region for  $\text{H}_2\text{O}_2$ ,  $\text{HCOOH}$ , and HMHP for the instrument used in this study.

chemical name (abbrev.)	chemical formula	MS stage	Ion <i>m/z</i>	ionic composition	quantification method	water dependence
water vapor	H <sub>2</sub> O	1 1	104 121	<sup>13</sup> CF <sub>3</sub> O·(H <sub>2</sub> O) <sup>-</sup> CF <sub>3</sub> O·(H <sub>2</sub> O) <sub>2</sub> <sup>-</sup>	FT-IR FT-IR	v. strong v. strong
acetic acid (AA)	CH <sub>3</sub> C(O)OH	1 2	79 145 → 79	HF·[O(O)CCH <sub>3</sub> ] <sup>-</sup> CF <sub>3</sub> O·[AA] <sup>-</sup> → HF[O(O)CCH <sub>3</sub> ] <sup>-</sup>	gravimetric gravimetric	strong strong
formic acid	HC(O)OH	1	65	HF·(O(O)CH) <sup>-</sup>	gravimetric	strong
nitric acid	HNO <sub>3</sub>	1	82	HF·(ONO <sub>2</sub> ) <sup>-</sup>	gravimetric	weak
peracetic acid (PAA)	CH <sub>3</sub> C(O)OOH	1	161	CF <sub>3</sub> O·(PAA) <sup>-</sup>	colorimetric (UV-Vis)	moderate
hydrogen peroxide	HOOH	1 2	119 119 → 85	CF <sub>3</sub> O·(HOOH) <sup>-</sup> CF <sub>3</sub> O·(HOOH) → CF <sub>3</sub> O <sup>-</sup>	colorimetric (UV-Vis) colorimetric (UV-Vis)	strong strong
methyl hydro- peroxide (MHP)	CH <sub>3</sub> OOH	2	133 → 85	CF <sub>3</sub> O·(CH <sub>3</sub> OOH) <sup>-</sup>	colorimetric (UV-Vis)	strong
hydroxymethyl hydroperoxide (HMHP)	HOCH <sub>2</sub> OOH	1	149	CF <sub>3</sub> O·(HMHP) <sup>-</sup>	FT-IR	weak
hydroxy-acetone (HAC)	HOCH <sub>2</sub> C(O)CH <sub>3</sub>	1	159	CF <sub>3</sub> O·(HAC) <sup>-</sup>	gravimetric	weak
glycolaldehyde (GLYC)	HOCH <sub>2</sub> C(O)H	2	145 → 85	CF <sub>3</sub> O·(GLYC) <sup>-</sup> → CF <sub>3</sub> O <sup>-</sup>	FT-IR	weak

Table E.2: Detection and quantification of compounds using negative-ion CF<sub>3</sub>O<sup>-</sup> CIMS.

Scheme S1: Model mechanism at T = 295 K and P = 1 atm, based on a condensed version of Figure E.4 in the main text. The OH chemistry of cyclohexane (CHX) is monitored as it produces RO<sub>2</sub> and consumes HO<sub>2</sub>. Standard background chemistry (e.g. HO<sub>x</sub>, NO<sub>y</sub> reactions, not shown) is also incorporated. Minor oxygenated organics (e.g. 1-hydroperoxy-2-oxybut-3-ene) are all lumped as a generic "product" compound. Rate coefficients for the background reactions are based off IUPAC recommendations except where noted.

### *Ozonolysis Mechanism*

$$x_{34POZ} = 0.6;$$

$$x_{12POZ} = 0.4;$$

$$x_{MACR} = 0.68;$$

$$x_{MACROO} = 1 - x_{MACR};$$

$$x_{synMACROO} = 0.2;$$

$$x_{antiMACROO} = 0.8;$$

$$x_{MVK} = 0.42;$$

$$x_{MVKOO} = 1 - x_{MVK};$$

$$x_{synMVKOO} = 0.6;$$

$$x_{antiMVKOO} = 0.4;$$

$$x_{dioxole} = 0.25;$$

$$x_{dioxirane} = 0.72;$$

$$x_{stable} = 0.03;$$

$$x_{decarbox} = 0.7;$$

$$x_{PA\_CH_3CH_2} = 0.35;$$

$$x_{HP} = 0.3;$$

$$x_{DC} = 0.3;$$

$$x_{RO} = 0.4;$$

$$x_{OH} = x_{12POZ} \cdot x_{MVKOO} \cdot x_{synMVKOO};$$

$$y_{OH} = x_{OH} \dots$$

$$+ x_{OH} \cdot x_{RO} + x_{OH} \cdot x_{DC} + x_{OH} \cdot x_{RO} \cdot x_{RO} \dots$$

$$+ x_{34POZ} \cdot x_{MACROO} \cdot x_{antiMACROO} \cdot x_{dioxirane} \dots$$

$$\cdot x_{decarbox} \cdot x_{RO} \cdot x_{PA\_CH_3CH_2} \dots$$

$$+ x_{34POZ} \cdot x_{MACROO} \cdot x_{synMACROO} \cdot x_{dioxirane} \dots$$

$$\cdot x_{decarbox} \cdot x_{RO} \cdot x_{PA\_CH_3CH_2} \dots$$

$$+ x_{12POZ} \cdot x_{MVKOO} \cdot x_{antiMVKOO} \cdot x_{dioxirane} \dots$$

$$\cdot x_{decarbox} \cdot x_{RO} \cdot x_{PA\_CH_3CH_2};$$

$$y_{form} = (x_{34POZ} \cdot x_{MACROO} + x_{12POZ} \cdot x_{MVKOO}) \dots$$

$$+ x_{OH} \cdot x_{RO} + x_{OH} \cdot x_{RO} \cdot x_{RO} \dots$$

$$+ x_{34POZ} \cdot x_{MACROO} \cdot x_{antiMACROO} \cdot x_{dioxirane} \cdot x_{decarbox} \dots$$

$$+ x_{34POZ} \cdot x_{MACROO} \cdot x_{synMACROO} \cdot x_{dioxirane} \cdot x_{decarbox} \dots$$

$$+ x_{12POZ} \cdot x_{MVKOO} \cdot x_{antiMVKOO} \cdot x_{dioxirane} \cdot x_{decarbox};$$

$$y_{HO_2} = x_{OH} \cdot x_{DC} + x_{OH} \cdot x_{RO} \cdot x_{RO} \dots$$

$$+ x_{34POZ} \cdot x_{MACROO} \cdot x_{antiMACROO} \cdot x_{dioxirane} \cdot x_{decarbox} \dots$$

+ x34POZ.\*xMACROO.\*xsynMACROO.\*xdioxirane.\*xdecarbox;

y<sub>macr</sub> = x34POZ.\*xMACR;

y<sub>mvk</sub> = x12POZ.\*xMVK;

**Isop + O3;**

k = 1.3e-17;

Y(MACR) = y<sub>macr</sub>;

Y(MVK) = y<sub>mvk</sub>;

Y(HCHO) = y<sub>form</sub>;

Y(CH2OO\_SCI) = y<sub>macr</sub> + y<sub>mvk</sub>;

Y(MACROO\_SCI) = x34POZ.\*xMACROO.\*xstable;

Y(MVKOO\_SCI) = x12POZ.\*xMVKOO.\*xstable;

Y(OH) = y<sub>OH</sub>;

Y(HO2) = y<sub>HO2</sub>;

Y(products) = xOH\*xHP + xOH.\*xDC + xOH.\*xRO...  
 + x34POZ.\*xMACROO.\*xantiMACROO.\*xdioxole...  
 + x12POZ.\*xMVKOO.\*xantiMVKOO.\*xdioxole;

**MACR + O3;**

k = 1.8e-18;

Y(products) = 1;

**MVK + O3;**

k = 4.8e-18;

Y(products) = 1;

**Isop + OH;**

k = 1e-10;

Y(products) = 1;

**MACR + OH;**

k = 3.4e-11;

Y(products) = 1;

**MACR + OH;**

k = 1.9e-11;

Y(products) = 1;

**CHX + OH;**

k = 7.3e-12;

Y(CHX\_RO2) = 1;

**CHX\_RO2 + CHX\_RO2;**

k = 5.7e-12;

Y(cyclohexanone) = 0.5;

Y(cyclohexanol) = 0.5;

**CHX\_RO2 + HO2;**

$$k = 1.612e-11;$$

$$Y(\text{cyclohexane hydroperoxide}) = 1;$$

**CHX\_RO2 + SCI;**

$$k = 5e-12;$$

$$Y(\text{products}) = 1;$$

**CH2OO\_SCI + H2O;**

$$k = 0.9e-15;$$

$$Y(\text{HMHP}) = 0.73;$$

$$Y(\text{H}_2\text{O}_2) = 0.06;$$

$$Y(\text{HCHO}) = 0.06;$$

$$Y(\text{HCOOH}) = 0.21;$$

**CH2OO\_SCI + (H2O)2;**

$$k = 0.8e-12;$$

$$Y(\text{HMHP}) = 0.40;$$

$$Y(\text{H}_2\text{O}_2) = 0.06;$$

$$Y(\text{HCHO}) = 0.06;$$

$$Y(\text{HCOOH}) = 0.54;$$

**CH2OO\_SCI + Isop;**

$$k = 1.78e-13;$$

$$Y(\text{products}) = 1;$$

**CH2OO\_SCI + O3;**

$$k = 1e-12;$$

$$Y(\text{HCHO}) = 0.7;$$

**MACROO\_SCI + H2O;**

$$k = 1.8e-15;$$

$$Y(\text{products}) = 1;$$

**MACROO\_SCI;**

$$k = 250;$$

$$Y(\text{products}) = 1;$$

**MVKOO\_SCI + H2O;**

$$k = 1.8e-15;$$

$$Y(\text{products}) = 1;$$

**MVKOO\_SCI;**

$$k = 250;$$

$$Y(\text{products}) = 1;$$

***Background Mechanism***

**HO2 + HO2;** % water dependent, k based on Stone and Rowley PCCP 2005

$$k = 1.8e-14.*\exp(1500/T)*(1+1e-25.*fH2O.*M.*\exp(4670/T));$$

$$Y(H2O2) = 1;$$

$$Y(O2) = 1;$$

**OH + H2O2;**

$$k = 1.69e-12;$$

$$Y(H2O) = 1;$$

$$Y(HO2) = 1;$$

**OH + HO2;**

$$k = 1e-10;$$

$$Y(H2O) = 1;$$

$$Y(O2) = 1;$$

**OH + OH;**

$$k0 = 7.0e-31.*(T/300).^(-1);$$

$$kinf = 2.6e-11.*(T/300).^(-0);$$

$$Fc = 0.6;$$

$$k = (k0.*M)/(1+(k0.*M./kinf)).*Fc.^((1+(\log10(k0.*M./kinf)).^2).^(-1));$$

$$Y(H2O2) = 1;$$

**OH + HONO;**

$$k0 = 7.0e-31.*(T/300).^(-1);$$

$$kinf = 2.6e-11.*(T/300).^(-0);$$

$$Fc = 0.6;$$

$$k = (k0.*M)/(1+(k0.*M./kinf)).*Fc.^((1+(\log10(k0.*M./kinf)).^2).^(-1));$$

$$Y(H2O) = 1;$$

$$Y(H2O2) = 1;$$

**OH + HNO3;**

$$k0 = 2.4e-14*\exp(460/T);$$

$$k2 = 2.7e-17*\exp(2199/T);$$

$$k3 = 6.5e-34*\exp(1335/T);$$

$$k = k0+k3.*M./(1+k3.*M./k2);$$

$$Y(H2O) = 1;$$

$$Y(NO3) = 1;$$

**OH + NO;**

$$k0 = 7.0e-31.*(T/300).^(-2.6);$$

$$kinf = 3.6e-11.*(T/300).^(-0.1);$$

$$k = k0.*M./(1+(k0.*M./kinf)).*0.6.^((1+(\log10(k0.*M./kinf)).^2).^(-1));$$

$$Y(HONO) = 1;$$

**OH + NO2;**

$$k0 = 1.51e-30.*(T/300).^(-3.0);$$
 % Updated to Mollner, Science, 2010

$$kinf = 2.58e-11.*(T/300).^(-0.0);$$

$$k = k0.*M./(1+(k0.*M./kinf)).*0.6.^((1+(\log10(k0.*M./kinf)).^2).^(-1));$$

$$Y(\text{HNO}_3) = 1;$$

**OH + NO<sub>2</sub>;**

$$k_0 = 6.2\text{e-}32 \cdot (T/300)^{-3.9};$$

$$k_{\text{inf}} = 8.1\text{e-}11 \cdot (T/300)^{-0.5};$$

$$k = k_0 \cdot M / (1 + (k_0 \cdot M / k_{\text{inf}})) \cdot 0.6^{((1 + (\log_{10}(k_0 \cdot M / k_{\text{inf}}))^2)^{-1})};$$

$$Y(\text{HOONO}) = 1;$$

**HOONO;**

$$eq = 3.9\text{e-}27 \cdot \exp(10125/T);$$

$$k_0 = 6.2\text{e-}32 \cdot (T/300)^{-3.9};$$

$$k_{\text{inf}} = 8.1\text{e-}11 \cdot (T/300)^{-0.5};$$

$$k_f = k_0 \cdot M / (1 + (k_0 \cdot M / k_{\text{inf}})) \cdot 0.6^{((1 + (\log_{10}(k_0 \cdot M / k_{\text{inf}}))^2)^{-1})};$$

$$k = k_f / eq;$$

$$Y(\text{HO}) = 1;$$

$$Y(\text{NO}_2) = 1;$$

**HO<sub>2</sub> + NO;**

$$k = 8.17\text{E-}12;$$

$$Y(\text{OH}) = 1;$$

$$Y(\text{NO}_2) = 1;$$

**O(3P) + HO<sub>2</sub>;**

$$k = 5.9\text{e-}11;$$

$$Y(\text{OH}) = 1;$$

$$Y(\text{O}_2) = 1;$$

**O(3P) + O<sub>2</sub>;**

$$k = 6.0\text{e-}34 \cdot (T/300)^{-2.4} \cdot M;$$

$$Y(\text{O}_3) = 1;$$

**O<sub>3</sub> + HO<sub>2</sub>;**

$$k = 1.9\text{e-}15;$$

$$Y(\text{OH}) = 1;$$

$$Y(\text{O}_2) = 2;$$

**O<sub>3</sub>+OH;**

$$k = 7\text{e-}14;$$

$$Y(\text{HO}_2) = 1;$$

$$Y(\text{O}_2) = 1;$$

**O(1D) + H<sub>2</sub>O;**

$$k = 2\text{e-}10;$$

$$Y(\text{OH}) = 2;$$

**O(1D);**

$$k = 3.2\text{e-}11 \cdot \exp(67/T) \cdot M;$$

$$Y(\text{O}_3\text{P}) = 1;$$

**O(3P) + NO;**

$$k_0 = 9.0e-32 \cdot (T/300)^{-1.5};$$

$$k_{inf} = 3.0e-11 \cdot (T/300)^{-0.0};$$

$$k = k_0 \cdot M / (1 + (k_0 \cdot M / k_{inf})) \cdot 0.6^{((1 + (\log_{10}(k_0 \cdot M / k_{inf}))^2)^{-1})};$$

$$Y(\text{NO}_2) = 1;$$

**O(3P) + NO<sub>2</sub>;**

$$k = 1.04e-11;$$

$$Y(\text{NO}) = 1;$$

$$Y(\text{O}_2) = 1;$$

**O(3P) + NO<sub>2</sub>;**

$$k_0 = 2.5e-31 \cdot (T/300)^{-1.8};$$

$$k_{inf} = 2.2e-11 \cdot (T/300)^{-0.7};$$

$$k = k_0 \cdot M / (1 + (k_0 \cdot M / k_{inf})) \cdot 0.6^{((1 + (\log_{10}(k_0 \cdot M / k_{inf}))^2)^{-1})};$$

$$Y(\text{NO}_3) = 1;$$

**O<sub>3</sub> + NO;**

$$k = 1.86e-14;$$

$$Y(\text{NO}_2) = 1;$$

$$Y(\text{O}_2) = 1;$$

**O<sub>3</sub>+NO+NO;**

$$k = 2e-38 \cdot c_{\text{O}_2};$$

$$Y(\text{NO}) = 1;$$

$$Y(\text{NO}_3) = 1;$$

**O<sub>3</sub> + NO<sub>2</sub>;**

$$k = 3.46e-11;$$

$$Y(\text{NO}_3) = 1;$$

$$Y(\text{O}_2) = 1;$$

**NO<sub>3</sub> + NO<sub>2</sub>;**

$$k_0 = 2.7e-27 \cdot (T/300)^{-4.4};$$

$$k_{inf} = 1.4e-12 \cdot (T/300)^{-0.7};$$

$$k = k_0 \cdot M / (1 + (k_0 \cdot M / k_{inf})) \cdot 0.6^{((1 + (\log_{10}(k_0 \cdot M / k_{inf}))^2)^{-1})};$$

$$Y(\text{N}_2\text{O}_5) = 1;$$

**N<sub>2</sub>O<sub>5</sub> + H<sub>2</sub>O;**

$$k = 2.5e-22;$$

$$Y(\text{HNO}_3) = 2;$$

**N<sub>2</sub>O<sub>5</sub> + H<sub>2</sub>O + H<sub>2</sub>O;**

$$k = 1.8E-39 \cdot f_{\text{H}_2\text{O}} \cdot M;$$

$$Y(\text{HNO}_3) = 2;$$

$$Y(\text{H}_2\text{O}) = 1;$$

**N2O5;**

$$eq = 2.7e-27 * \exp(11000./T);$$

$$k0 = 9.0e-29 * (T./300).^(-4.4);$$

$$kinf = 1.4e-12 * (T./300).^(-0.7);$$

$$kf = k0 * M. / (1 + (k0 * M. / kinf)) * 0.6.^((1 + (\log_{10}(k0 * M. / kinf)).^2).^(-1));$$

$$k = kf / eq;$$

$$Y(NO3) = 1;$$

$$Y(NO2) = 1;$$

**NO3 + NO;**

$$k = 2.27e-11;$$

$$Y(NO2) = 2;$$

**NO3 + NO3;**

$$k = 2.1e-16;$$

$$Y(NO2) = 2;$$

$$Y(O2) = 1;$$

**NO3 + HO2;**

$$k = 3.5e-12;$$

$$Y(NO2) = 1;$$

$$Y(O2) = 1;$$

$$Y(OH) = 1;$$

**HO2 + NO2;**

$$k0 = 2.0e-31 * (T./300).^(-3.4);$$

$$kinf = 2.9e-12 * (T./300).^(-1.1);$$

$$k = k0 * M. / (1 + (k0 * M. / kinf)) * 0.6.^((1 + (\log_{10}(k0 * M. / kinf)).^2).^(-1));$$

$$Y(HO2NO2) = 1;$$

**HO2NO2;**

$$eq = 2.1e-27 * \exp(10900/T);$$

$$k0 = 2.0e-31 * (T./300).^(-3.4);$$

$$kinf = 2.9e-12 * (T./300).^(-1.1);$$

$$kf = k0 * M. / (1 + (k0 * M. / kinf)) * 0.6.^((1 + (\log_{10}(k0 * M. / kinf)).^2).^(-1));$$

$$k = kf / eq;$$

$$Y(HO2) = 1;$$

$$Y(NO2) = 1;$$

**OH + HO2NO2;**

$$k = 4.71e-12;$$

$$Y(HO2) = 1;$$

$$Y(NO2) = 1;$$

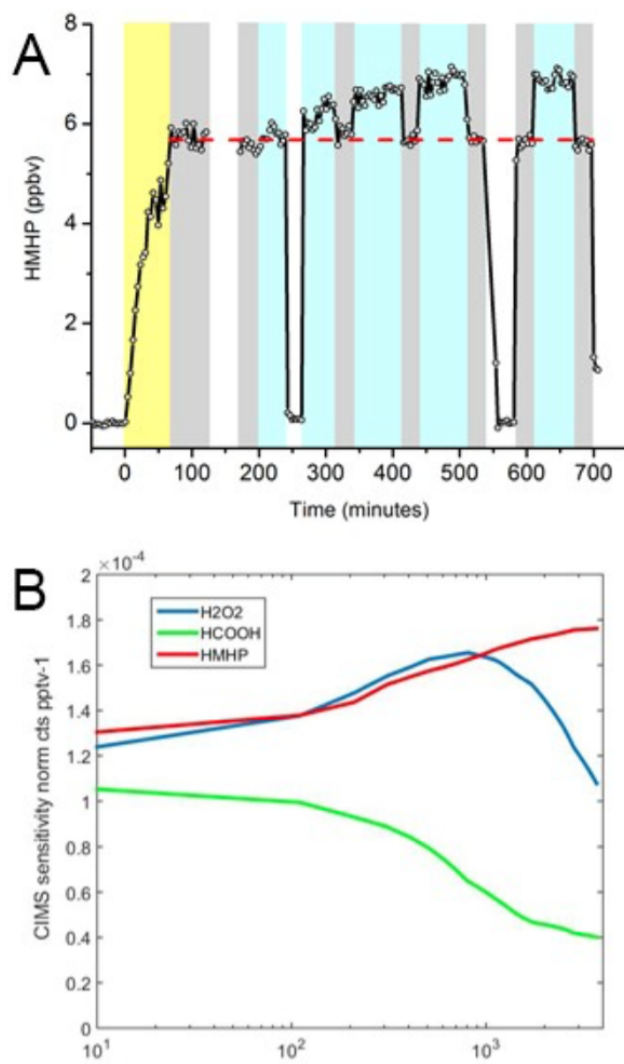


Figure E.10: Wall loss rates of HMHP, HCOOH, and H<sub>2</sub>O<sub>2</sub> at two representative relative humidity conditions.

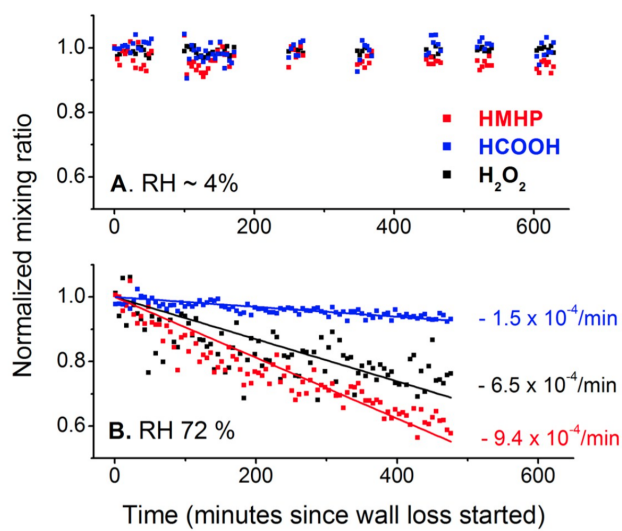


Figure E.11: An ozonolysis experiment, where formic acid was injected halfway through the experiment. The signal for HPMF was the only one (besides formic acid) that increased due to the reaction of  $\text{CH}_2\text{OO} + \text{HCOOH}$ .

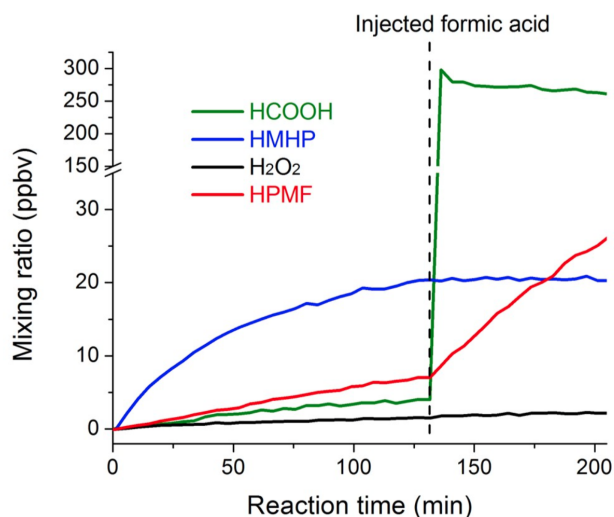


Figure E.12:  $\text{CF}_3\text{O}^-$  CIMS mass spectra shown for three RH experiments. In general acidic compounds are quantified by their fluoride transfer ( $\text{M} + \text{F}^-$ ) ion and most other compounds by the cluster ion ( $\text{M} + \text{CF}_3\text{O}^-$ ). Each compound has a water-dependent calibration that has not been applied to the figure, so the ion signals should be interpreted qualitatively. The peak labels correspond to: (a)  $\text{HCOOH}$  –  $m/z$  65 (transfer) and  $m/z$  131 (cluster), (b)  $\text{H}_2\text{O}_2$  –  $m/z$  119 (cluster), (c) Glycolaldehyde or isobaric compound –  $m/z$  145 (cluster), (d) HMHP –  $m/z$  149 (cluster), (e) Hydroxyacetone or methylvinylhydroperoxide –  $m/z$  159 (cluster), (f) Unidentified –  $m/z$  171, (g) HPMF –  $m/z$  177 (cluster), (h) Unidentified –  $m/z$  191, (i) Unidentified –  $m/z$  217, (j) Acetic acid –  $m/z$  79 (transfer) and  $m/z$  145 (cluster), (k) Methyl hydroperoxide –  $m/z$  133 (cluster). Peaks from  $\text{CF}_3\text{O}$  reagent have been subtracted and suspected impurities are not labelled. Glycolaldehyde and acetic acid cluster ( $m/z$  145) are isobaric; however, the  $m/z$  145 signal is mainly due to glycolaldehyde at low RH and acetic acid at higher RH (confirmed by a corresponding transfer ion).

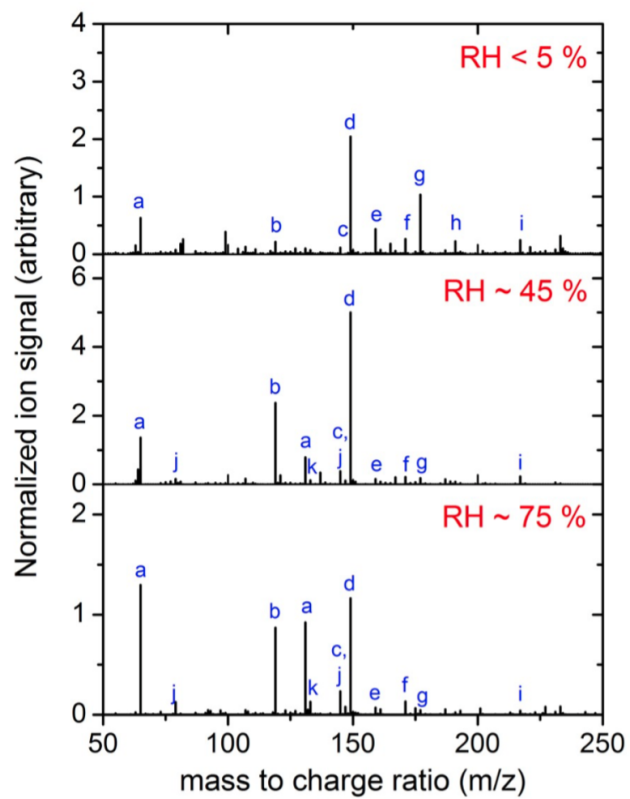


Figure E.13: Possible rearrangement of dioxiranes with allylic functionality.

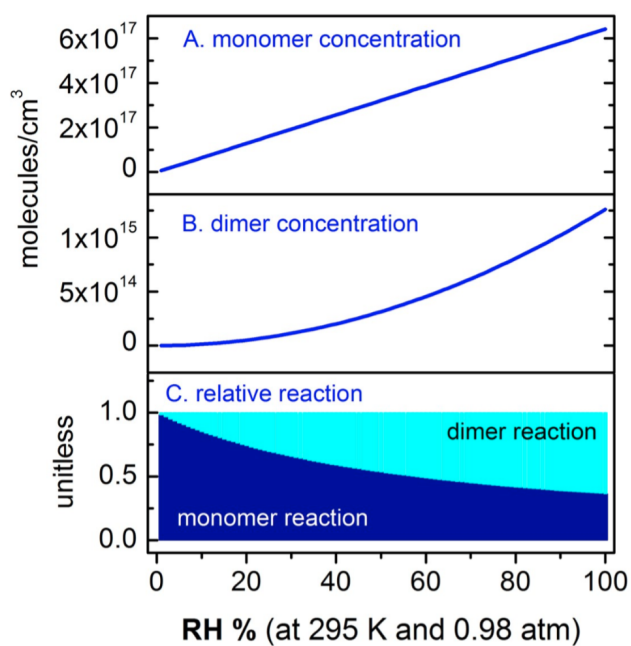


Figure E.14: The population of (A) water monomer molecules and (B) water dimer molecules as a function of RH, based on cluster association equilibrium thermodynamic functions reported in Owicki *et al.* (1975). The fraction of each reaction, using rate coefficients reported in the main text and in the Supporting Information, is shown in panel C.

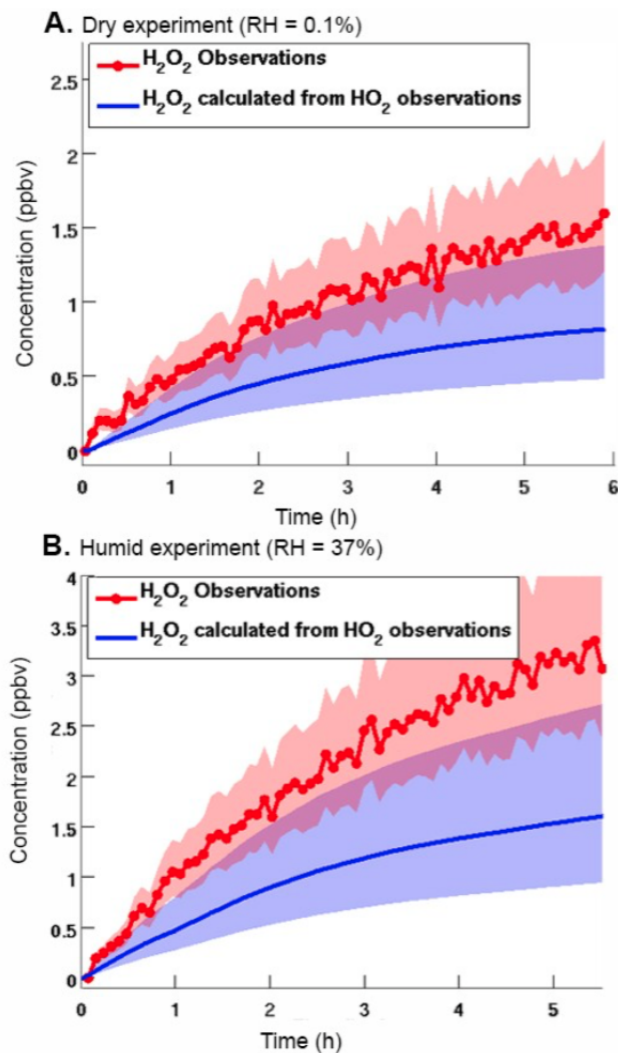
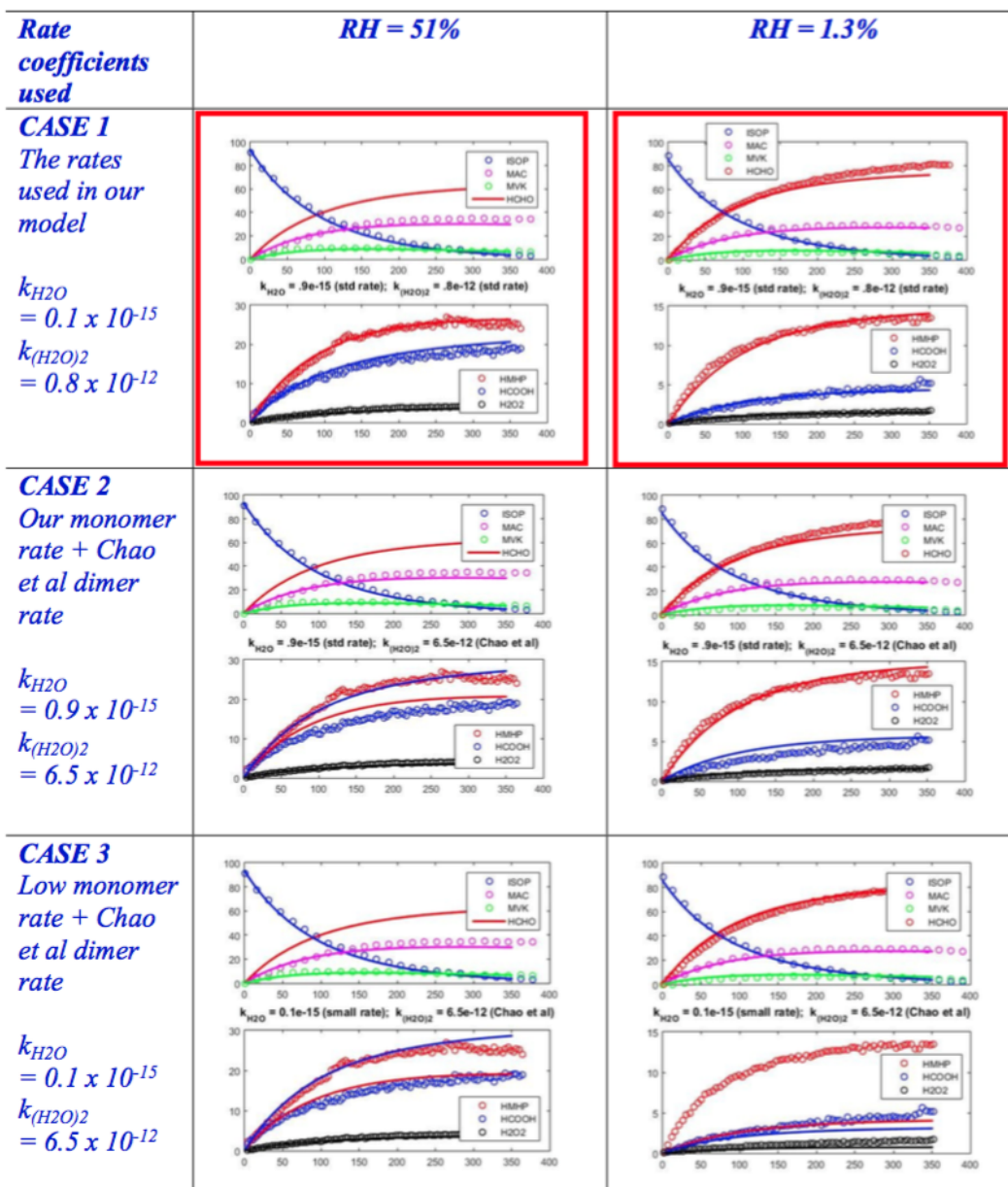


Figure E.15: Comparison between H<sub>2</sub>O<sub>2</sub> observed by CIMS (filled markers) and calculated H<sub>2</sub>O<sub>2</sub> using observed HO<sub>2</sub> data from GTHOS (Figure E.17, lines) for (A) dry conditions,  $k_{HO_2+HO_2,295K} = 2.92 \times 10^{-12} \text{ cm}^3 \text{ molec}^{-1} \text{ s}^{-1}$  and (B) RH 37% conditions,  $k_{HO_2+HO_2,295K} = 3.53 \times 10^{-12} \text{ cm}^3 \text{ molec}^{-1} \text{ s}^{-1}$ . Uncertainty bounds are used as reported in the main text. Rate coefficients are derived from the temperature and RH dependence reported by Stone and Rowley (2005).



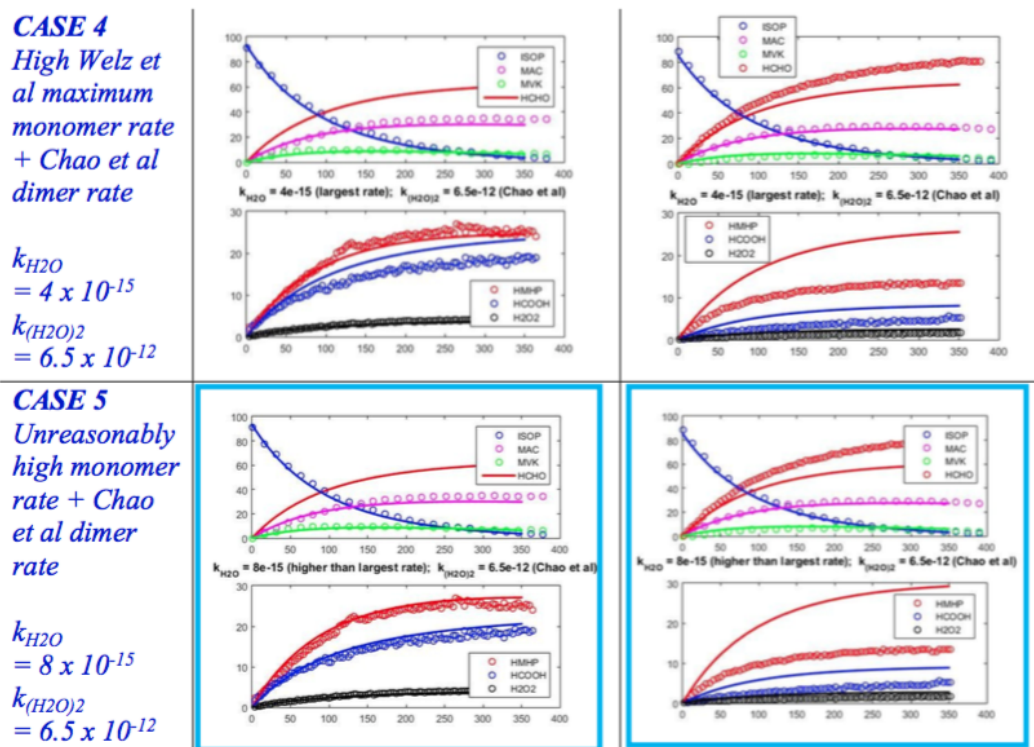


Figure E.16: Model sensitivity study using two RH conditions (RH = 51%, where the water dimer and water monomer rate are both important, and RH = 1.2%, where only the water monomer rate is important). Results from 5 sensitivity cases, using different monomer and dimer rate coefficients, are shown. Case 1, shown in the red border, successfully reproduces all data reported in this work (Figure E.5 in the manuscript). Cases 2-5 explored the dimer rate coefficient of Chao *et al.* (2015). For the Chao *et al.* (2015) dimer rate coefficient to reproduce the RH = 51% results, the monomer rate coefficient would need to be adjusted to be higher than the upper bound reported by Welz *et al.* (2012) – shown in the blue border, Case 5. The high monomer rate in Case 5 now over predicts CH<sub>2</sub>OO water products in the dry case.

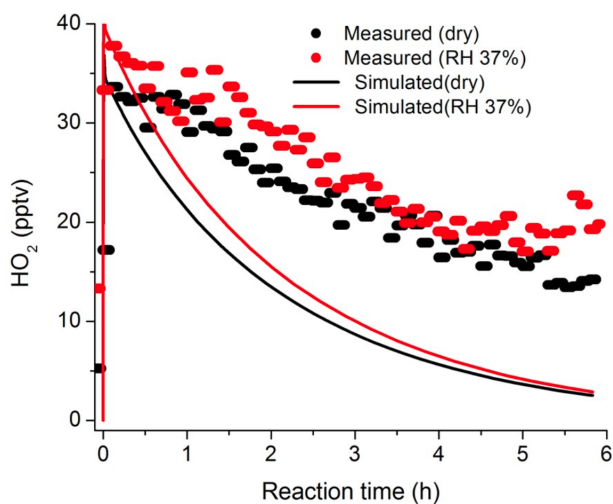


Figure E.17: Simulated and measured  $\text{HO}_2$  mixing ratios at two RH conditions during the FIXCIT campaign. The model mechanism does not yet include second-generation sources of  $\text{HO}_2$ .

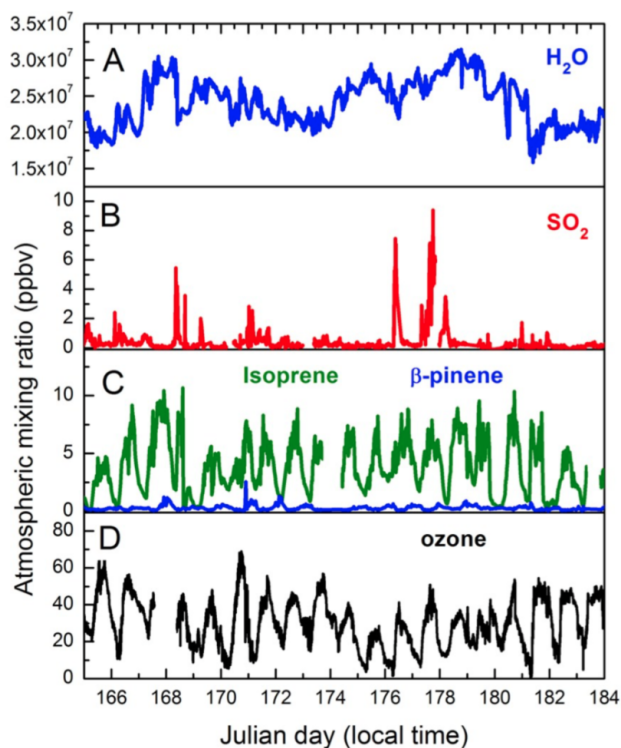


Figure E.18: Atmospheric mixing ratios of (A) water vapor, (B) sulfur dioxide, (C) exocyclic VOCs isoprene and  $\beta$ -pinene, and (D) ozone during the measurement period of the SOAS campaign.

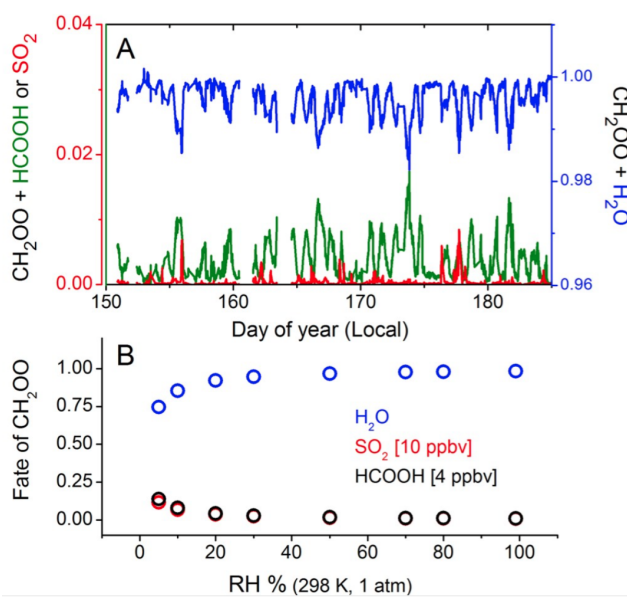


Figure E.19: (A) Fraction of  $\text{CH}_2\text{OO}$  that reacts with  $\text{H}_2\text{O}$ ,  $\text{SO}_2$  and  $\text{HCOOH}$  during the SOAS campaign. (B) Given high  $\text{SO}_2$  and  $\text{HCOOH}$  mixing ratios, the fate of  $\text{CH}_2\text{OO}$  varies with RH; however, the  $\text{H}_2\text{O}$  reaction dominates at all realistic atmospheric humidities.